

ABSTRACT

Title of Document: DEBRIS CATALOG AUGMENTATION PROJECT:
PRIORITIZATION AND COORDINATION OF
THE OBSERVATIONS

Ignacio E. Viciano Semper, Master of Science, 2017

Directed by: Professor Raymond J. Sedwick

Department of Aerospace Engineering

The Two-Line Element sets are a data format in which the information about all the largest Earth-orbiting objects is encoded. Published by the North American Aerospace Defense Command (NORAD), the TLE files are used along with a simplified perturbation model, such as the SGP4, in order to obtain the position and velocity of the objects at a given time. This project seeks to develop the necessary tools to enhance the TLEs for Earth orbiting debris using the cooperation of the Amateur Astronomer community, as increasing the amount of information will reduce the errors due to the propagation of the orbits along time. For that, several geometrical constraints are applied: to be seen, the observation must occur at nighttime and the object illuminated by the Sun and at a reasonable elevation. It has been calculated how, for 13,309 satellites of a given TLEs file, 380 were able to be observed from a selected position and epoch. Errors from the propagator are a concern, so historical data of a large collection of objects has been processed, showing how the main inaccuracies of the SGP4 model occur in the velocity direction and for high altitude orbits. To make sure that a particular object is captured, statistical analysis of historical data will be used to coordinate different observations.

DEBRIS CATALOG AUGMENTATION PROJECT: COORDINATION AND
PRIORITIZATION OF THE OBSERVATIONS

By

Ignacio E. Viciano Semper

Thesis submitted to the Faculty of the Graduate School of the University of
Maryland, College Park, in partial fulfillment of the requirements for the
degree of Master of Science

2017

Advisory Committee:

Professor Raymond J. Sedwick

@ Copyright by
Ignacio E. Viciano Semper
2017

Acknowledgements

I would like to thank Dr. Raymond Sedwick for giving me the opportunity of developing this research project under his advisement. Without him it would have been difficult to find such an interesting topic to work with.

Thanks also to the University of Maryland for letting me do a fantastic exchange year in one of the best universities of the country, I have learnt a lot.

Finally, thanks to Elizabeth Warner, coordinator of the University of Maryland Observatory, for her guidance and assistance with making preliminary observations for this project.

Contents

List of Tables	v
List of Figures	vi
1 Introduction	1
1.1 Motivation	1
1.2 Concept Overview	3
1.3 Prioritization and Coordination of the Observations	4
2 Theoretical Background	6
2.1 Two Line Element sets	6
2.2 SGP4 model	7
3 Geometric Constraints	9
3.1 Basic constraints	9
3.2 Coordinate Systems	11
3.3 Observability Calculations	13
4 Observation considerations	16
4.1 Calibration process	16
4.2 Astronomer Hardware	17

4.3	Debris filtering	19
4.4	Preliminary observations	21
4.5	Problems with the observations	26
5	Cooperative targeting	28
5.1	Preliminary analysis	28
5.2	Statistical analysis	31
5.2.1	Introduction	31
5.2.2	Global results	36
5.2.3	Type of orbit	41
6	Final Platform	45
6.1	Main folder	45
6.2	Geometry folder	47
6.3	SGP4_files folder	47
6.4	TLE_files_storage folder	47
6.5	Historical_TLE	49
7	Conclusions and Future Work	51

List of Tables

1	Description of Line 1 of a TLE set.	7
2	Description of Line 2 of a TLE set.	7
3	Brightness of different bodies and satellites.	23
4	Objects #1,000, 4,864 and 30,000 information	33
5	Number of objects that pass the filters applied to the character- istic ellipses.	37
6	Number of objects in the catalog per type of orbit.	42
7	Average error for each type of orbit.	42

List of Figures

1	Growth of the Satellite catalog since first launch to space cite-celestrak.	2
2	Flow structure for the SGP4 model [3], where each rectangular box is function implemented with MATLAB in the case of this project.	8
3	Schematic of the geometric constrains for an object observability.	10
4	Spherical coordinate system (Azimuth-Altitude)	12
5	Equatorial coordinate system	12
6	Important position vectors of the scenario.	14
7	Earth shadow constraint representation.	15
8	Representation of the FOV of the telescope in the first and last moments of the position calibration.	17
9	In blue, satellites from the June 12th 2017 TLE file propagated to 21:00:00 UTC of June 13th 2017. In orange, observable objects from the University of Maryland Observatory at that time. . . .	19
10	In blue, satellites from the June 12th 2017 TLE file propagated to 21:00:00 UTC of June 13th 2017. In orange, observable objects from Valencia, Spain, at that time.	20

11	The UMD observatory during one of the sessions.	22
12	Long exposure example in the computer of the telescope, which is used to set the observations.	22
13	Long exposure image from the UMD Observatory of the pass of the SL-8 rocket body, #7434 of the NORAD catalog.	24
14	Long exposure image from the UMD Observatory of the pass of a Delta 2 rocket body.	25
15	Star background previous to the pass of the Delta 2 rocket body. The brightest stars are circled thanks to a postprocess of the image with the software ImageVIEWca.	25
16	Observation of an object almost falling outside the FOV.	27
17	Two-dimensional sketch that shows how the errors may differ greatly in the ECI frame even that a clear pattern is shown – the error tends to the center of the orbit.	29
18	RSW coordinates frame.	30
19	Debris object #30,000 of the catalog statistical analysis for a 5 year-period. Error between propagated and real positions in the RSW coordinates frame. 632 total TLE entries processed.	32
20	Characteristic ellipse of the debris object #30,000 of the catalog.	33
21	Debris object #1,000 of the catalog statistical analysis for a 5 year-period. Error between propagated and real positions in the RSW coordinates frame. 1,184 total TLE entries processed.	34
22	Characteristic ellipse of the debris object #1,000 of the catalog.	34
23	Debris object #4,864 of the catalog statistical analysis for a 5 year-period. Error between propagated and real positions in the RSW coordinates frame. 1,444 total TLE entries processed.	35

24	Characteristic ellipse of the debris object #4,864 of the catalog.	35
25	$\pm 2\sigma$ characteristic ellipses of 16,053 objects (almost all the current objects of the catalog).	36
26	$\pm 2\sigma$ characteristic ellipses after filtering really high errors.	38
27	$\pm 2\sigma$ characteristic ellipses after filtering the objects with less than 500 observations.	38
28	$\pm 2\sigma$ characteristic ellipses applying a combined filter that deletes high-error objects and less than 500 observations ones.	39
29	$\pm 2\sigma$ characteristic ellipses of objects with reasonable errors.	39
30	$\pm 2\sigma$ characteristic ellipses of objects with a maximum 1-FOV errors.	40
31	$\pm 2\sigma$ characteristic ellipses of LEO objects.	43
32	$\pm 2\sigma$ characteristic ellipses of MEO objects.	43
33	$\pm 2\sigma$ characteristic ellipses of HEO objects.	44

Chapter 1

Introduction

1.1 Motivation

The North American Aerospace Defense Command (NORAD), mainly through the Joint Space Operations Center (JSpOC), detects, tracks and identifies all manmade objects orbiting the Earth, which in the majority of cases are debris[1]. Other institutions such as the European Space Agency (ESA)¹ and the Roscosmos also have several programs for tracking space debris². However, the frequency of the observations is low, so the data is first recorded and then propagated in order to know the location of the debris at any given time and avoid possible dangers.

The information about the objects is contained in the Two-Line Element sets (TLE sets), which are files that the NORAD makes public and use two lines of ASCII characters to define the information of every object in terms of the mean orbital elements for a given epoch. The data provided by the TLE sets has to be used with an analytic general perturbation model to propagate the orbits along time, but there is always an error between the prediction and the reality, that can be critical. The purpose of this project is to enhance TLE data with the help of the Amateur Astronomers community, that is estimated to be 500,000 people³, providing the necessary interface and tools.

Since the launch of the first artificial satellite to space in 1957, Sputnik 1, more than 35,000 man-made objects have been cataloged by the JSpOC (Figure

¹http://www.esa.int/Our_Activities/Operations/Space_Debris/About_space_debris/

²<http://www.unoosa.org/pdf/pres/copuos2011/tech-33.pdf>

³<https://astrosociety.org/edu/resources/useduc06.html>

1), half of which decayed into the Earth’s atmosphere. Around 21,000 of them are currently being tracked, forecasted for possible conjunctions and analyzed to obtain data of interest. The size of the objects ranges from small 10 cm debris to enormous first stages of old rockets, and only a few of them are actually functioning payloads or satellites. The ephemeris data is distributed in the form of Two-Line Element sets. The TLEs are available and are distributed through the Space Track website (<https://www.space-track.org>). Celestrak[1] has been also used for this study. These files have to be used along with a perturbation model in order to propagate the state vector of the object to a desirable epoch. To propagate satellites using the TLEs requires use of the Simplified General Perturbations model SGP4, which takes into account several perturbation effects such as the Earth’s shape, atmospheric drag, radiation and gravitation effects from other bodies like the Sun or the Moon.

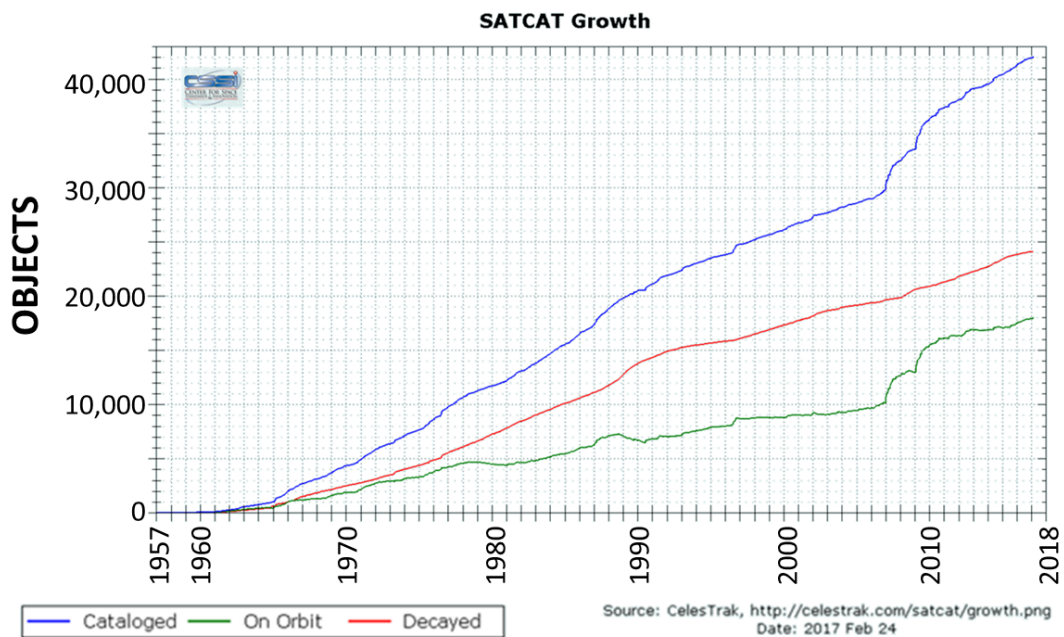


Figure 1: Growth of the Satellite catalog since first launch to space citecelestrak.

The precision of the data provided by the TLE sets degenerates with time due to several effects like the uncertainties in the atmospheric density and the perturbations from radiation. Moreover, the propagation method performs some approximations, so it is important to have the most accurate data for

a given epoch by updating the observations as frequently as possible. In the U.S. it is the Space Surveillance Network (SSN) who conducts periodic observations through a collection of different ground based sensors: radar, laser and optical systems. However, the resources are limited and the observations are not performed frequently enough, which translates into a significant divergence between real and predicted data, as it is demonstrated in the analysis that follows.

There are several websites where TLE data is published along with additional information and analysis and source code in different programming languages. Celestrak is maintained by the Center for Space Standards and takes the information provided by NORAD. It takes some supplemental TLE data directly from the owner or operator of some satellites, which highly improves the precision compared with the information provided by the SSN. Sadly, about 93% of the objects orbiting Earth are non-operational, so this supplemental data cannot be obtained.

1.2 Concept Overview

The optical imaging of low altitude debris is complicated because their velocity and the relatively low Field Of View (FOV) of the telescope mounting. High altitude orbits debris are better suited for optical observations, as the use of active radar is not possible and the velocity is much more smaller, giving a low angular rate viewed from the ground. As it will be discussed in this project, there is an uncertainty in the orbital parameters that may cause that the object falls outside the FOV when attempting an observation to the predicted position. Also, the slew rate of these systems is also typically too slow to be able to do a local search around the nominal direction.

However optical sensors, which basically are telescopes, are the most prevalent tool used, because of the interest of the Amateur Astronomy (AA) commu-

nity in observing the sky at night. As said, the AA community is estimated in around 500,000 people all over the world. This community has several interests, and some of them are already used to identify and track objects in Earth's orbit. An example of this can be found in the website of the SeeSat-L listserve ⁴, a site where Amateur Astronomers can exchange data and observations in order to keep tracking satellites and objects.

Given the level of interest to observe and track these objects, the current project seeks to provide this community with the necessary tools to collect, exchange and process this data more effectively, as well as allow others in the larger community with perhaps a more passing interest to get involved.

The final stage of the project will be creating a main interface to the community, possibly a dedicated website that will allow users to set up accounts, upload image data and access derived products. Raw image data will be archived and made freely available to the community for research purposes, as also all processing software. For those interested in algorithmic development, new codes could be uploaded for consideration as additions to the basic algorithm suite. Down the line, other interfaces such as dedicated mobile applications may be provided that will allow for interfacing with the data archive or to provide improved timing or geolocation data.

1.3 Prioritization and Coordination of the Observations

The Debris Catalog Augmentation Project has several areas that need to be developed: calibration methods for both the time and the position, programs and algorithms to process the observational scenario, image processing methods, web interface... In this thesis the focus has been the prioritization and coordination of the observations, which consists in the need of the project in coordinating observations and understanding the errors of the prediction models

⁴<http://www.satobs.org/seesat/>

in order to distribute observations to the available AA all over the world.

As a satellite drifts away from its predicted position, it can fall outside of the FOV of the telescope. Having multiple observers available to conduct observations over a period of time makes possible that several observation directions can be coordinated around the nominal direction with the objective of capturing the object in one of the images.

This cooperative targeting doesn't need to happen simultaneously or during the same orbit. For any given object a standardized information about the behavior of its position error between the predicted and real states can be implemented, using a maximum likelihood approach that may change based on the time since epoch. A first observer will be tasked with trying to view the object at the coordinates that target is most likely at whatever local observing time provides the best sun angle. If the object is found in this first observation, any future observations of the object will be canceled, but if it is not then the next most likely coordinates will be provided to the next observer, repeating the process until the object is found.

Since it is always nighttime somewhere on Earth and the dusk/dawn terminators move continuously across the Earth's surface, observers will be continuously becoming available, that will make possible to have an evolving list of participants, dynamic and reactive to each change in the participation list and with each object that is successfully imaged.

In this context, a historical analysis of the error between predicted and real positions of the cataloged objected will be done, in order to understand the characteristics of this error and what can be done to design observations avoiding repeated failures.

Chapter 2

Theoretical Background

2.1 Two Line Element sets

Two-Line Element sets are the data format through which the orbital elements of an object at a given epoch are given. The structure of the data is such that is suitable to be used with a perturbation model in order to be able to predict the position and velocity of the object for future instants. The data is stored in two lines of 80 ASCII characters, which have the following format:

```
1 NNNNU NNNNAAA NNNN.NNNNNNNN +.NNNNNNNN +NNNN-N +NNNN-N N NNNN  
2 NNNN NNN.NNNN NNN.NNNN NNNNNNN NNN.NNNN NNN.NNNN NN.NNNNNNNNNNNNN
```

As explained by Kelso (2004) [4], a space or a period can have no other character. N values may be any number between 0 and 9 or, in some cases, a space. A may be any letter from A to Z or a space. C represents the classification of the element set, which is normally a U for unclassified data. A “+” can either be a plus sign, a minus sign, or a space and “-” can either be a plus or minus sign.

Tables 1 and 2 show the meaning of each field.

Table 1: Description of Line 1 of a TLE set.

Field	Column	Description
1.1	1	Line Number of Element Data
1.2	3-7	Satellite Number
1.3	8	Classification
1.4	10-11	International Designator (Last two digits of launch year)
1.5	12-14	International Designator (Launch number of the year)
1.6	15-17	International Designator (Piece of the launch)
1.7	19-20	Epoch Year (Last two digits of year)
1.8	21-32	Epoch (Day of the year and fractional portion of the day)
1.9	34-43	First Time Derivative of the Mean Motion
1.10	45-52	Second Time Derivative of Mean Motion (decimal point assumed)
1.11	54-61	BSTAR drag term (decimal point assumed)
1.12	63	Ephemeris type
1.13	65-68	Element number
1.14	69	Checksum (Modulo 10)

Table 2: Description of Line 2 of a TLE set.

Field	Column	Description
2.1	1	Line Number of Element Data
2.2	3-7	Satellite Number
2.3	1-16	Inclination [Degrees]
2.4	18-25	Right Ascension of the Ascending Node [Degrees]
2.5	27-33	Eccentricity (decimal point assumed)
2.6	35-42	Argument of Perigee [Degrees]
2.7	44-51	Mean Anomaly [Degrees]
2.8	53-63	Mean Motion [Revs per day]
2.9	64-68	Revolution number at epoch [Revs]
2.10	69	Checksum (Modulo 10)

2.2 SGP4 model

The SGP4 model is the evolution of several previous studies, being first developed by Ken Cranford in 1970 and updated by Hoots, F.R., and Roehrich, R.L. [2], along with other propagators as the SDP4, SGP8 and SDP8, that are out of the scope of this project. The SGP4 was revised in 2004 by Vallado, D.A., et al [3]. These models were created specifically to work with the TLEs provided by the NORAD.

Hoots, F.R., and Roehrich, R.L. [2] implemented FORTRAN IV code for the

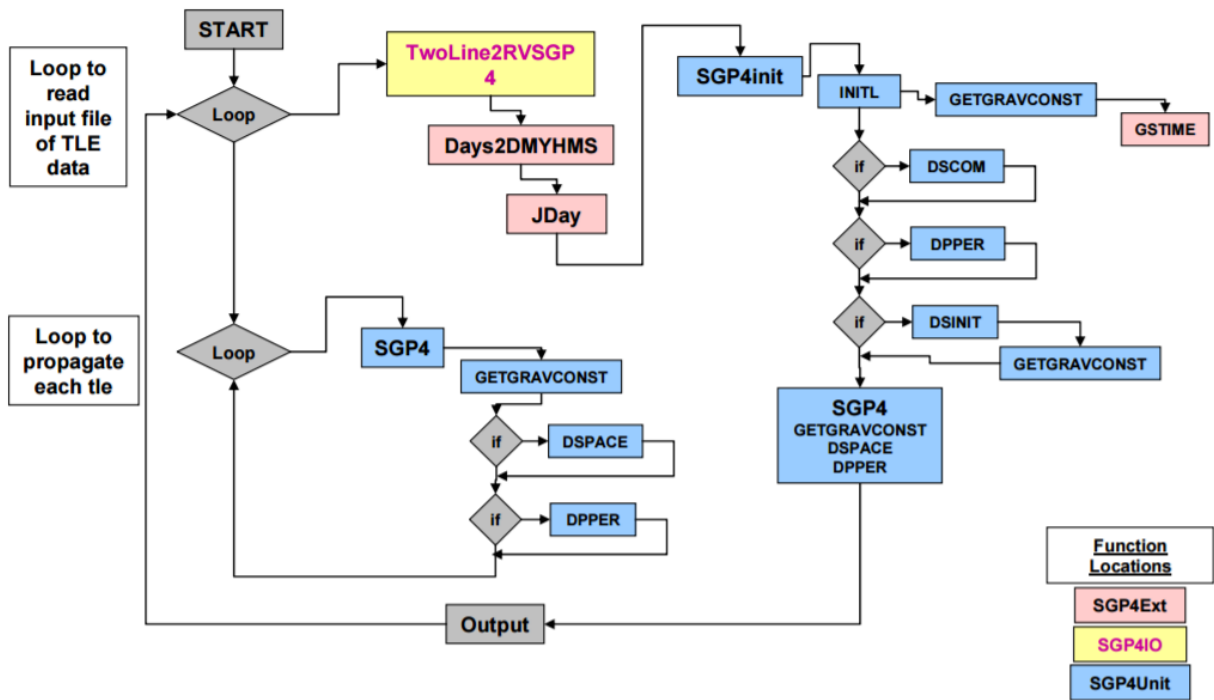


Figure 2: Flow structure for the SGP4 model [3], where each rectangular box is function implemented with MATLAB in the case of this project.

propagation, and Vallado [3] revisited and transformed it to *C++*. It requires more than 10 functions to use the propagator, which structure flow is shown in the Figure 2.

A MATLAB version of the code is used in this project. The SGP4 model considers the gravitational zonal harmonic effects J_2 , J_3 and J_4 , the drag (different routine for Near Earth objects or Deep Space), the radiation effects and the gravitational effect of the Moon and the Sun.

To take into account the atmospheric drag, the SGP4 model uses power density functions, that use the *BSTAR* drag term as the ballistic coefficient. Sometimes a negative *BSTAR* drag term is found, which implies that energy is added to the system. It is an error due to the limited SGP4 model of the force with respect the the dynamical environment.

Chapter 3

Geometric Constraints

3.1 Basic constraints

There are three basic geometric constraints that need to be taken into account in order to know if an object is observable in a particular epoch:

- The observation must be done in nighttime
- The object must be above the local horizon of the observer
- The object must be illuminated by the Sun

There are other two constraints that will be also applied but they depend on the telescope FOV and the spot where the observation is done:

- If two objects fall in the FOV at the same time it would be impossible to know which one is the targeted
- Observations with low elevation over the local horizon would be obstructed by trees, mountains, buildings, etc. so a minimum elevation must be considered

The final platform resulting from the project will take the observer position and the desired observation epoch, will propagate the debris position until that epoch and will filter the objects that don't satisfy the conditions described above.

Figure 3 illustrates the constraints of the problem.

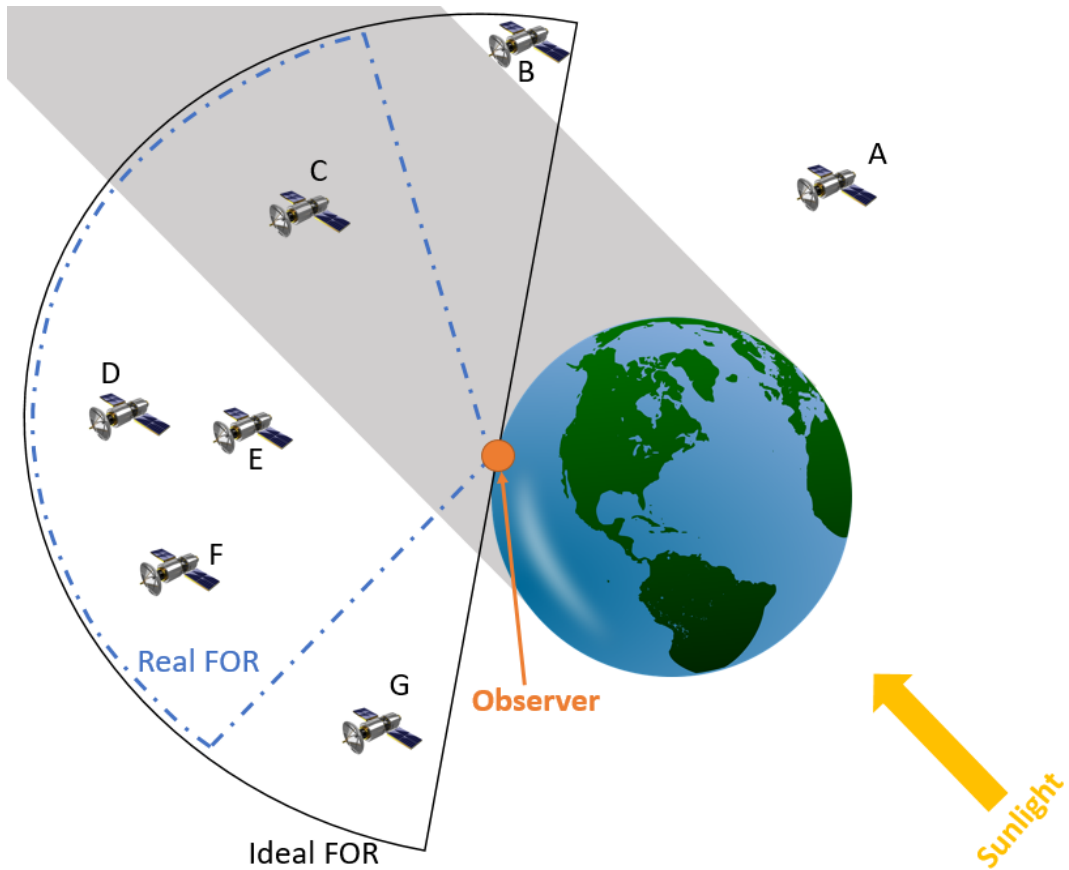


Figure 3: Schematic of the geometric constraints for an object observability.

The Figure reduces the scenario to two dimensions. The first constraint, that is that the observer is at night, is fulfilled. The semi-sphere delimited from the observer's local horizon is the ideal Field Of Regard (FOR), which corresponds to the second constraint. The Earth generates a cylindrical shadow that is shown in grey. Finally the ideal FOR is reduced because of a minimum elevation constraint giving the real FOR.

The situation of the seven objects of Figure 3 is the following, only object F will be suitable for an observation:

- Object A is outside the semi-sphere delimited by the local horizon, called ideal FOR, so it will not be suitable for an observation
- Object B is illuminated by the Sun and is in the ideal FOR, but because of an elevation constraint it falls outside the real FOR, so it will not be

selected for an observation

- Object C is in the ideal FOR but it is shadowed by the Earth, so it will not be observable
- Objects E and D are illuminated by the Sun and in the real FOR, but they will probably interfere in the FOV of the observation, so they are not suitable for the observation at that particular epoch
- Object F is in the real FOR and illuminated by the Sun, so it will be selected to be observed
- Object G is not observable because it falls outside the real FOR even though it is illuminated by the Sun, as Object A

3.2 Coordinate Systems

In order to make an observation, the observer position at a certain epoch will be transformed to the Earth Centered Inertial (ECI) frame, as the position of the debris in the catalog is given in this coordinate system. Then, when a particular object is selected for the observation, the observer will need to be provided with the Right Ascension (RA) and Declination (DEC) of the object, as the telescopes usually work with these two coordinates.

There are two main ways of describing the position of an orbital object or celestial body.

The first one is based on the perpendicular plane to the Earth at the observer's location (Figure 4), and it is usually used in naked eye observations. The two coordinates used are the Azimuth and the Altitude, both expressed in degrees. The Azimuth is measured from the geographic north (N) and the altitude from the local horizon. As said before, this system is normally used in visual observations because high accuracy is not needed and the observer can more or

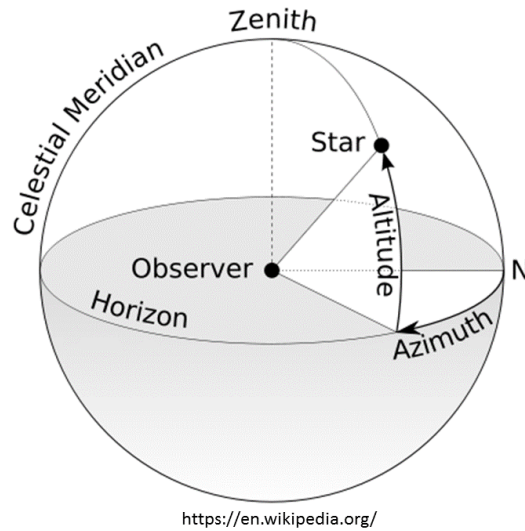


Figure 4: Spherical coordinate system (Azimuth-Altitude)

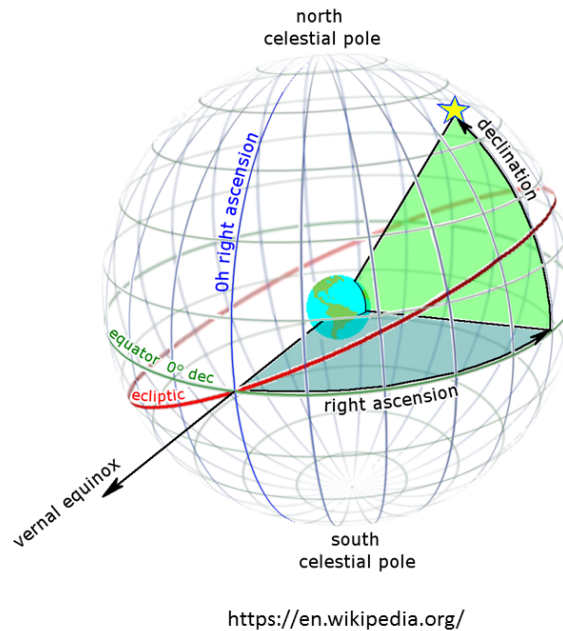


Figure 5: Equatorial coordinate system

less guess the position of a star or orbital object. An example where this coordinate system is useful is the observation of the Iridium flares, a phenomenon that only lasts few seconds consequence of the reflection onto the Earth surface of the antennas of an Iridium communication satellite.

The second way, which is the one used by the AA community is based on the Equatorial coordinate system. The reference for the Right Ascension node

is the vernal equinox, which is the x axis of the ECI frame, and the reference for the Declination is the equatorial plane, which is the plane generated by the x and y axis. The advantage of this coordinate system is that the RA and DEC of the stars, which are the most observed bodies of the sky, is fixed, so they can be used as references. The disadvantage is that, as the Earth rotates, the telescope needs to rotate at the same time in order to keep a particular RA-DEC pointing. The majority of the telescopes have two main rotation axes that allow to keep a RA-DEC pointing, using a computer or a device such as the *Setting circles*, very common among the AA community.

The orbital debris that are the target objects for this project move fast and are not as far away to be considered in the celestial sphere, where the stars are. Then, they don't have a constant RA-DEC coordinates, so for a given epoch they need to be calculated. With the vector between the observer and object in ECI coordinates, x and y can be used to obtain the local RA. The RA is expressed in hours:minutes:seconds. Then, using the magnitude of the vector and the z component the DEC can be obtained. The DEC is expressed in degrees:minutes:seconds.

3.3 Observability Calculations

To calculate if the object is inside the ideal FOR we do the scalar product between the observer position vector and the object/observer vector. The angle α obtained must be greater than the elevation threshold set:

$$\alpha_{FOR} = \arccos \left(\frac{\vec{r}_{obs} \cdot \vec{r}_{obj/obs}}{|\vec{r}_{obs}| |\vec{r}_{obj/obs}|} \right) \quad (1)$$

The position of the object is already given in the ECI frame through the SGP4 propagation, but the observer position is usually given as a longitude-latitude-elevation, which is the Earth Centered Earth Fixed (ECEF) coordinate

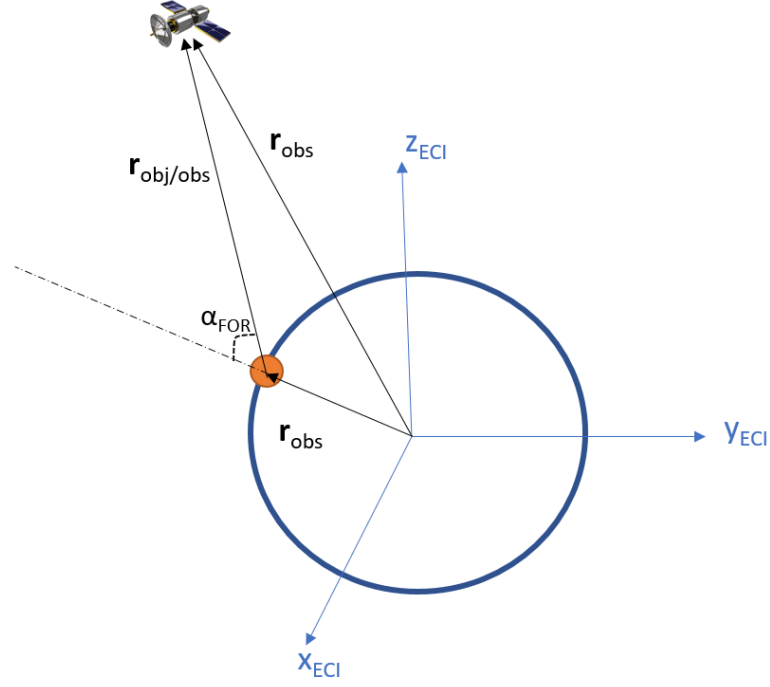


Figure 6: Important position vectors of the scenario.

system. A function already developed for MATLAB by Darin Koblick in 2010¹ is used to perform this operation. The function needs as an input the Julian day of the epoch and the ECEF coordinates of the observer, and outputs its ECI position vector.

Finally, using an algorithm developed by Hall [6] the Sun can be located relative to the Earth in order to apply the Earth's shadow constraint. It uses the following equations:

$$T_{UT1} = \frac{JD_{UT1} - 2,451,545.0}{36,525}$$

$$\lambda_{Sun} = 280.4606184^\circ + 36,000.7705361 \cdot T_{UT1}$$

$$M_{Sun} = 357.5277233^\circ + 35,999.05034 \cdot T_{UT1}$$

$$\lambda_{ecliptic} = \lambda_{Sun} + 1.914666471^\circ \sin M_{Sun} + 0.918994643 \sin(2M_{Sun})$$

$$\epsilon = 23.439291^\circ - 0.0130042 \cdot T_{UT1}$$

¹*ECEFtoECI.m* by Darin Koblick

$$\vec{r}_{Sun} = \begin{bmatrix} \cos \lambda_{ecliptic} \\ \cos \epsilon \cdot \sin \lambda_{ecliptic} \\ \sin \epsilon \cdot \sin \lambda_{ecliptic} \end{bmatrix} \quad (2)$$

And again, once the vector that points to the Sun from the center of the Earth is found, the dot product is used to obtain the angle between the Sun and the position vector of the satellite. Then, the distance D has to be calculated, and if it is bigger than the radius of the Earth, the satellite is illuminated by the Sun.

Again, applying some trigonometric relations we can find the distance of the object to the Sun-Earth vector and check if it is greater than the Earth's radius, which would mean that the object is illuminated by the Sun (Figure 7):

$$\gamma_{sun-obj} = \arccos \left(\frac{\vec{r}_{earth/sun} \cdot \vec{r}_{obj}}{|\vec{r}_{earth/sun}| |\vec{r}_{obj}|} \right) \quad (3)$$

$$distance = r_{obj} \sin(\gamma_{sun-obj}) \quad (4)$$

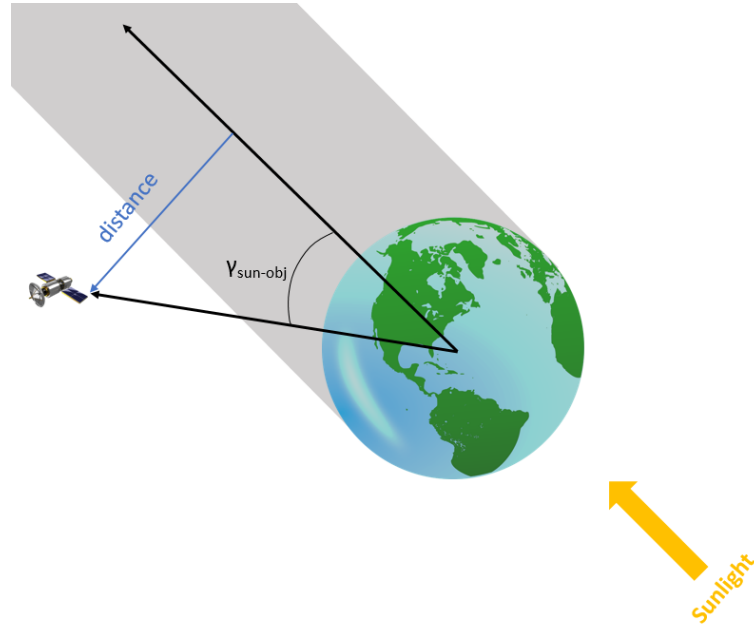


Figure 7: Earth shadow constraint representation.

Chapter 4

Observation considerations

4.1 Calibration process

Before an observation is done, the astronomer needs to calibrate the instruments in order to correct the position error. The time accuracy is another issue that also needs the calibration to be corrected.

The position error can be calibrated using a bright star, which is the usual method. As the telescope rotates to look for different targets some inaccuracies occur and provoke that the RA-DEC it is supposedly pointing is not exactly the corrects RA-DEC. Before an observation the observer will point to a bright star close to the target RA-DEC location, and will manually rotate the telescope to ensure that the target star falls into the center of the FOV, as at the first moment the star will probably not be in the center of the image. Then, as the RA-DEC of the star are known the observer can reset the telescope knowing exactly the current pointing.

This process is illustrated in Figure 8.

Ideally the best calibration would be done using a high quality camera, high precision telescope axis and a GPS receiver to have the best time accuracy, but it is not probable that a normal amateur astronomer have all of this, especially the GPS receiver, which would solve the time calibration problem.

A possible method of calibrating the time is using the GPS satellites but in a different way. As the position of this satellites are known with a high accuracy for any given epoch (within 1 cm), and their high altitude makes the

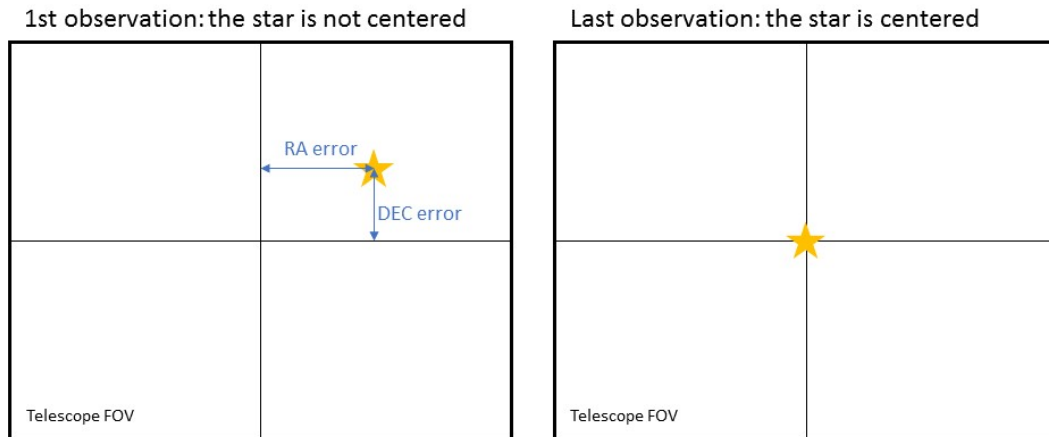


Figure 8: Representation of the FOV of the telescope in the first and last moments of the position calibration.

angular rate at which they cross the sky is slow, the observation of a passage at a particular epoch could be compared with the real position data of the satellite in order to see the advancement or delay at which the observation was done. As there are always several GPS satellites in the FOR of any observer this calibration method could always be done if the brightness of the satellite for the given observation is enough.

4.2 Astronomer Hardware

There are different methods, techniques and instruments that the Amateur Astronomy community uses to look at the sky, as the interests and possibilities of each person are diverse. Some of them just use naked eye to observe the stars and other celestial bodies, some use binoculars to have a better focus on particular targets while still having a large FOV and others use telescopes, with a wide range of power, quality and complementary devices.

This projects is meant for the astronomers that use telescopes with cameras attached to them, so they can record the pass of debris objects and the images can be processed. An order of magnitude of a usual telescope-camera mounting of an amateur astronomer is around 30 arcmin, but it varies in both directions (the FOV is usually a rectangle) and depends a lot on the camera.

Mentioned before, the *setting circles* mount is usually attached to the rotation axes of the telescope in order to follow a particular RA-DEC over time. The *setting circles* device can be digital and computerize, having databases of thousands celestial objects at which the telescope is able to point automatically. *GoTo telescopes* are also a popular option that a lot of AA use, which are computerized telescopes that can also automatically rotate to keep a particular RA-DEC or an astronomical object.

Charge-Coupled Device (CCD) cameras are widely use to record the observations, but other type of imaging such as webcams, DSLRs, photometry or spectroscopy are also used. CCDs have a quantum efficiency of 100%, linear outputs and are easy to use, which make them suitable for astronomic observation in the UV-to-infrared spectra, being the most popular imaging method among the AA community.

CCD images often have altered pixels due to imperfections, thermal noise or cosmic rays, whose effect can be calibrated out taking several exposures with the shutter opened and close and comparing the results.

Common GPS devices are used to know the coordinates of the observer with accuracy, and more advanced ones are also available to have a better precision of both position and time.

The internet has became an important tool for the AA community. There are a lot of user-maintained websites where images are shared and observations are coordinated, help and advice is provided and discussions are held in forums. Tools such as Clear Sky¹ help the astronomers in planning their observing sessions, because the weather is an important factor.

The Heavens Above website² is another important tool for the AA and has also been used in this project. One of the capabilities of the website is selecting a particular satellite, such as a GPS, Iridium or a debris object of the catalog,

¹<http://www.cleardarksky.com/>

²<http://www.heavens-above.com/>

and getting the visible time period from an observer position, the coordinates in both Azimuth-Altitude and RA-DEC coordinates, the brightness (if known), the path over the star background and more information. It has been useful to compare the results obtained in the project and check the code generated.

4.3 Debris filtering

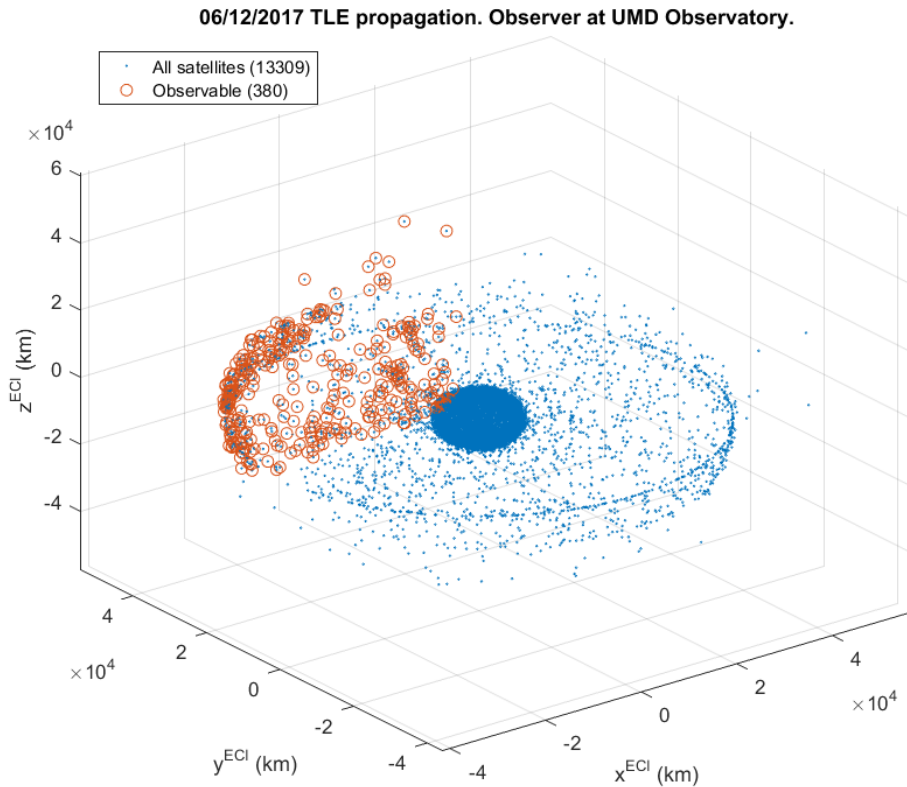


Figure 9: In blue, satellites from the June 12th 2017 TLE file propagated to 21:00:00 UTC of June 13th 2017. In orange, observable objects from the University of Maryland Observatory at that time.

The geometric problem is applied to the June 12th 2017 TLE file, that has 42,910 lines, which means 21,455 entries. Not all of them are different satellites, as a given satellite can be seen several times since the last TLE update and all the observations are recorded: around 8,100 measurements are actually updates from the objects already contained in the TLE file. Then, taking the most recent observation for each satellite the program starts with 13,355 satellites, marked

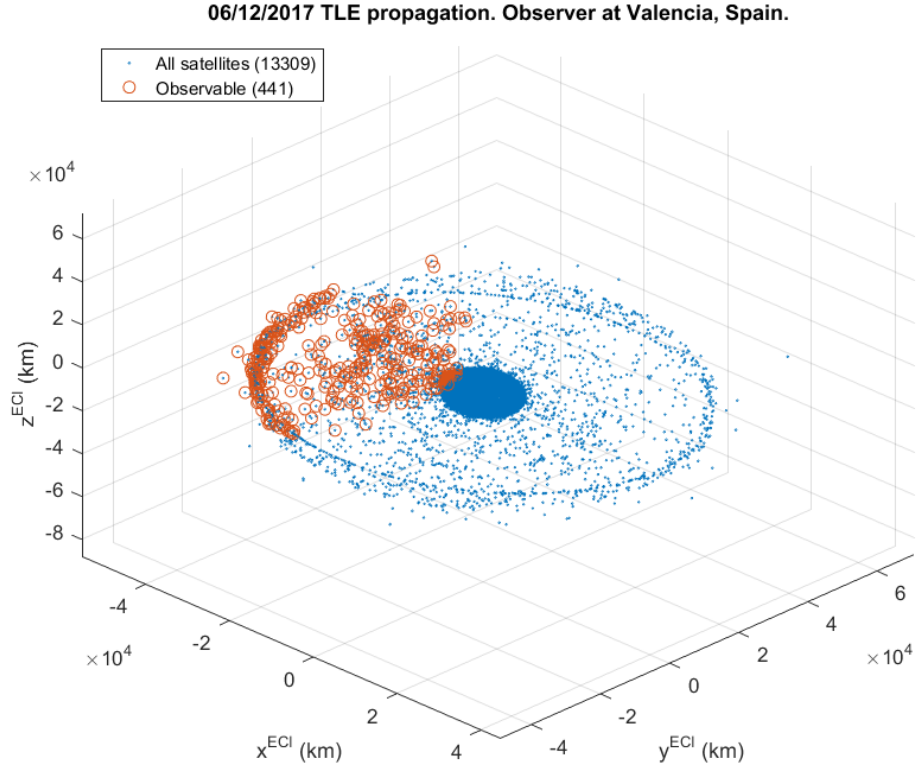


Figure 10: In blue, satellites from the June 12th 2017 TLE file propagated to 21:00:00 UTC of June 13th 2017. In orange, observable objects from Valencia, Spain, at that time.

in blue in Figures 9 and 10. These are not all the objects in the catalog, but are the ones contained in the TLE file of that particular day, as there are objects that are not seen every day.

The position of the observer is set at 2 locations, keeping the same UTC time of observation at 21:00:00 UTC of June 13th 2017:

- The University of Maryland Observatory, with coordinates 39.0020°N , 76.9561°W and an altitude of 53 m (Figure 9).
- The city of Valencia, Spain, with coordinates 39.4811°N , -0.3411°W and an altitude of 5 m (Figure 10).

Applying the geometric constraints explained in the previous chapter, taking into account a minimum elevation of 30 degrees, a total of 380 objects are visible

from Maryland and 441 from Valencia, taking into account a considered FOV of 30 arcmin for the interference between objects, that might make the observation fail appearing several objects in the same picture, making impossible to identify them.

This analysis shows how there will always be a big set of objects suitable to be observed, which is one of the premises of the project, and also shows how different locations all around the world have different geometric constraints that cause that not the same objects are observable at different locations.

4.4 Preliminary observations

An important part in the project are real observations, because the algorithms can be checked, AA scenarios can be reproduced and practical problems with the hardware systems show up so solutions can be found. This project has had a practical part that has been done at the University of Maryland (UMD) observatory.

The telescope used is a 152mm f/9 Astro-Physics refractor. Two different cameras were used. The main camera is a Santa Barbara Instrument Group (SBIG) ST-10 CCD camera, that mounted on the telescoped resulted in a 37.3x25.1arcmin FOV. The other camera, a Point Grey Grasshopper Express ADVS, is smaller but it is able to take much more frames per seconds, obtaining videos of the observations. With this small camera the FOV is 18.2x13.7arcmin. Figures 11 and 12 show the UMD observatory, with some of the computer-driven telescopes and how the computer looks when doing an observation.

As explained in the next chapter, to catch a debris object in an observation is not easy due to the uncertainty in its position. Another issue that was confirmed in the sessions in the observatory was that the brightness, which is usually unknown for debris objects, is also a key factor when trying to observe an object. Because of these two reasons not many successful observations were

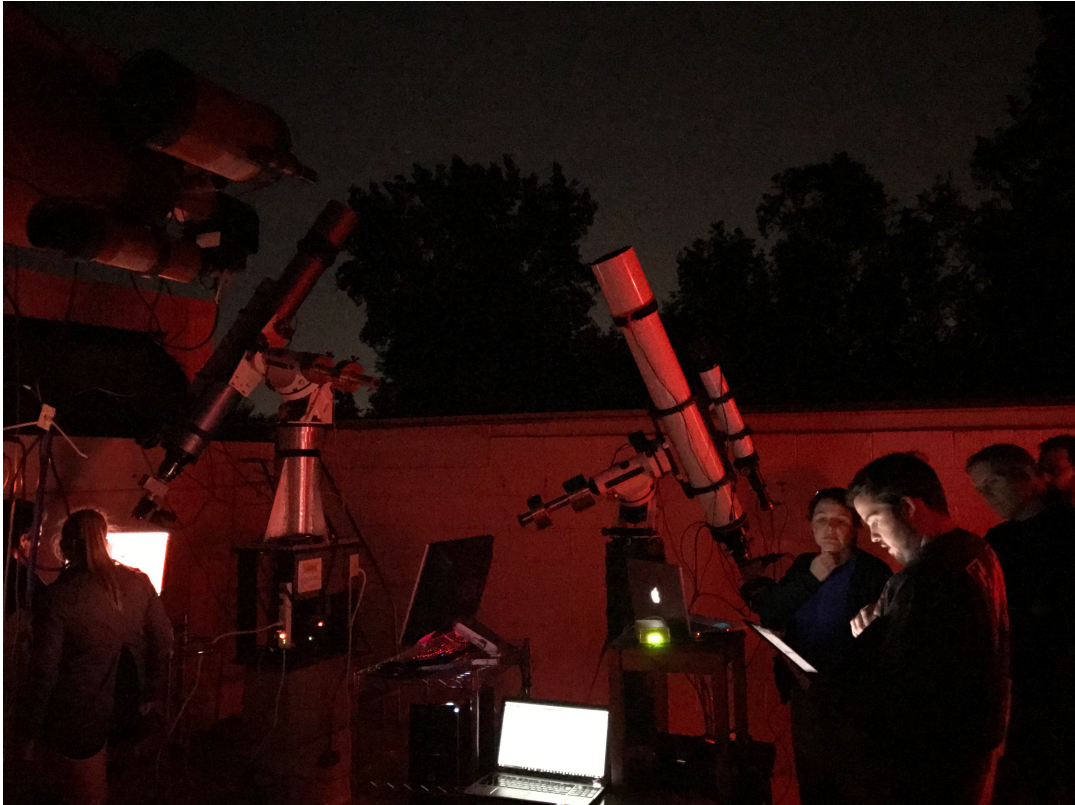


Figure 11: The UMD observatory during one of the sessions.

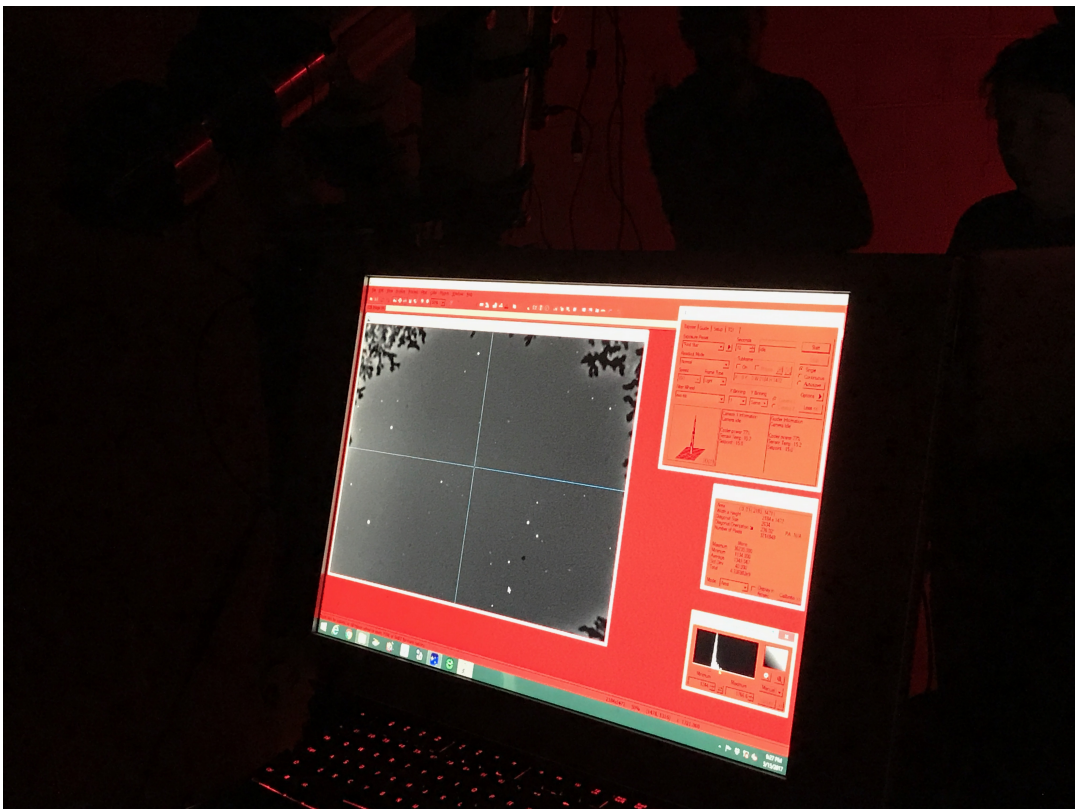


Figure 12: Long exposure example in the computer of the telescope, which is used to set the observations.

achieved, but a lot was learned.

The brightness of an object depends on several factors, such as the material of the object, its geometry and its position, and it is expressed with the magnitude, which uses a logarithmic scale. As lower is the value of the magnitude the brighter is the body that is observed. High magnitudes correspond to dim bodies. In Table 3 they are shown different values of different bodies.

Table 3: Brightness of different bodies and satellites.

Body	Apparent magnitude
Sun	-27
Full moon	-13
Venus	-5
Sirius (brightest star)	-1.5
Satellite flares	up to -9
ISS	up to -6
Bright satellite debris	around 3.5

Throughout the observations in the observatory it has been seen how object with brightness values higher than 10 are really difficult to observe, and even with lower values it is difficult.

This stage of the project still is in the preliminary phase. Some pictures have been taken, as the one shown in Figure 13. It is a 60 second long exposure image, taken in the University of Maryland Observatory with a CCD camera and a telescope with a FOV of 37.5 x 25.1 arcmin in that configuration. The object is called Cosmos 676, ID 7433 of the NORAD Catalog. It was launched in 1974 and its orbit is an almost circular LEO with a period of 100.52 min and an inclination of 74.05°.

Analyzing the background and knowing the time of the observation leads to obtain the coordinates of the object at that given time, which could then be processed in a TLE increasing the frequency of observations of the catalog, which is the main purpose of the project.

Figure 14 is a frame from a video taken with the second camera (ADVS) of the debris Delta 2 rocket body (#25876 of the NORAD catalog). The video



Figure 13: Long exposure image from the UMD Observatory of the pass of the SL-8 rocket body, #7434 of the NORAD catalog.

was recorded at 7.5 fps, giving an exposure time of 0.133 seconds. The star in the middle of the FOV is Mirfak (Alpha Persei). The brightness magnitude given by Heavens Above for that observation was 2.9, which is really good for a manmade object (see Table 3).

Figure 15 is a frame previous to the pass of the object. Looking at the initial image is difficult to see more stars a part from the central Mirfak, but processing the image with a specialized software, such as ImageVIEWwca in this case, can lead to obtain more stars in order to locate the object.



Figure 14: Long exposure image from the UMD Observatory of the pass of a Delta 2 rocket body.

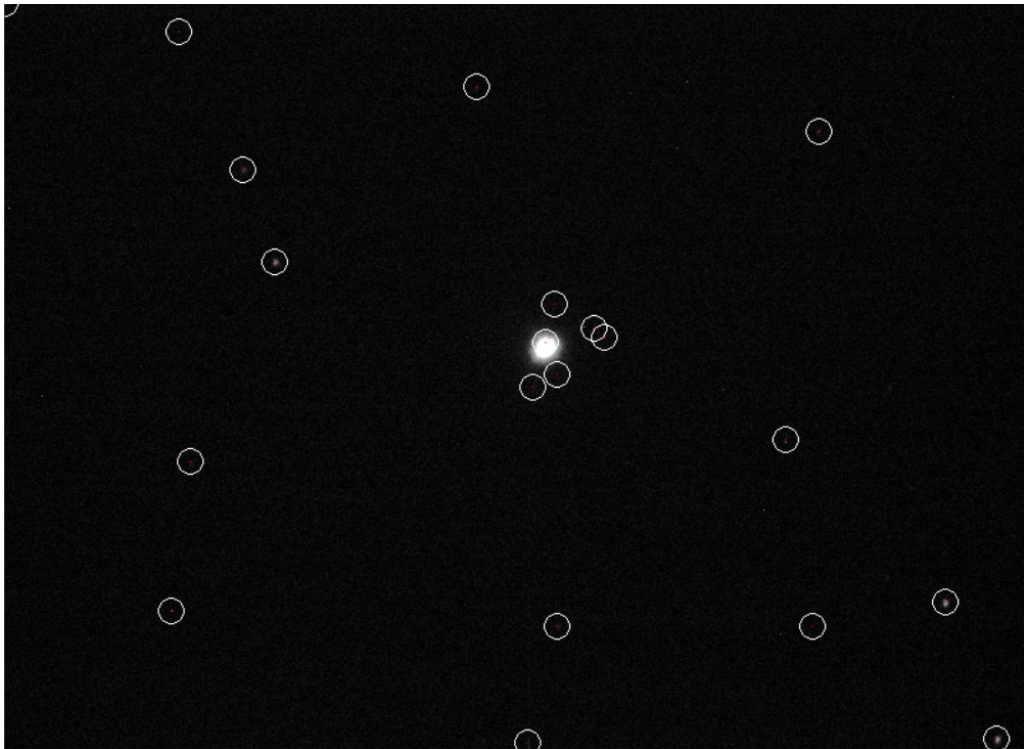


Figure 15: Star background previous to the pass of the Delta 2 rocket body. The brightest stars are circled thanks to a postprocess of the image with the software ImageVIEWWca.

4.5 Problems with the observations

It has been difficult to get successful observations in the observatory: more or less 50% of the tries, taking into account that most of the observations were selected using bright objects using Heavens Above.

One of problems is the accuracy of the objects data, which will be analyzed in the next chapter. The error is enough to provoke that the observation fails, even though the telescope is pointing perfectly to the predicted position at the given epoch.

Another problem is the calibration. The telescope was calibrated for every observation using a bright star near the target RA-DEC, but when calibrating for the next observation it was seen that just a couple of rotations could lead to a small decalibration, which could contribute to a failure. The time was calibrated using a GPS clock which had a high accuracy.

The third important issue about doing a correct observation was the brightness of the satellite. When looking to bright satellites from Heavens Above the success ratio was much higher than when looking to random objects, the majority of them with an unknown brightness magnitude. In the real application of this project the brightness would remain an unknown, what would be an important problem that needs to be solved.

The geometry is also important, as some times the object crosses the FOV in one of the corners, due to some of the inaccuracies mentioned before. If this happens the time and duration of the exposure becomes crucial as the object passes through the FOV quickly, as it happened in the observation shown in Figure 16. It was recorded using the video camera at 15 fps (66 ms of exposure time) and it only appeared in 2 frames, almost becoming a failed observation.

Processing the image and taking into account the characteristics of the exposure, duration of the observation and the background position, the position

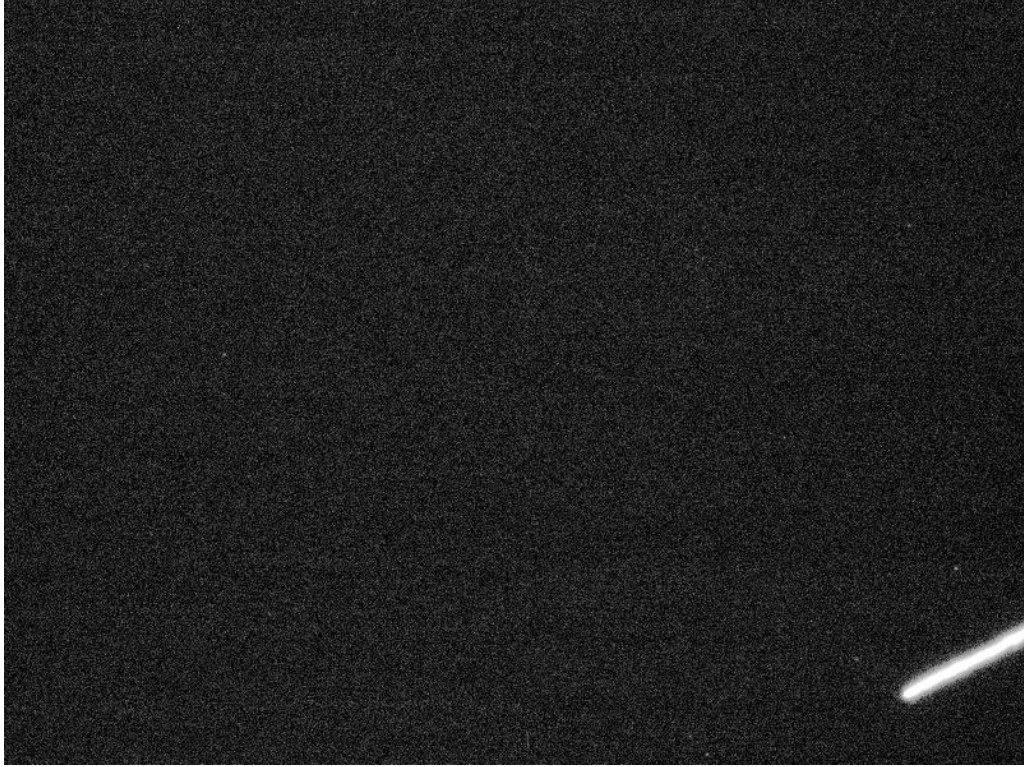


Figure 16: Observation of an object almost falling outside the FOV.

and velocity can be obtained. One of the requisites to perform this process is having the beginning or the end of the streak, because if the streak extends the full way across the image, then it is impossible to relate position and time. When deciding the length of the exposure there is a compromise between a longer exposure that helps to catch the object but has the danger of having it crossing the hole FOV or a shorter exposure with which you can ensure that the streak will not cross completely the FOV but makes more difficult to catch the object due to the uncertainties. The situation of Figure 16 is a limit situation where the exposure was short enough to catch the object and the end/beginning of the streak even the difficulty because its relative position in the FOV.

Chapter 5

Cooperative targeting

5.1 Preliminary analysis

As the elapsed time since the epoch of a particular TLE set increases, higher errors between the predicted position and the real position of an object will occur. This drift may cause the object to fall outside the Field of View (FOV) of the telescope when the astronomer points to the predicted position. The cooperative targeting will be a feature of the system with which several Amateur Astronomers available for a period of time will make coordinated observations in order to catch an object.

The measurements in a cooperative targeting process don't need to be simultaneous or at the same location on the Earth; a study has been done in order to make the process time-independent and able to update when an observation fails. The first observer would point the telescope to the most likely position of the object at that epoch, and if the object is found the next observations will be canceled, providing the system new targets to the remain observers available. If the object is not observed at first, statistical data analysis would be used to give the next astronomer a set of coordinates where the object is presumed to be based on the first failure. It is always nighttime somewhere in the Earth, so there will be continuously AAs available ready to receive new coordinates to look at, making the cooperative targeting a dynamic and ideally uninterrupted process.

Several websites such as the mentioned Space Track and Celestrak provide historical data of the unclassified objects in Earth's orbit. This historical data

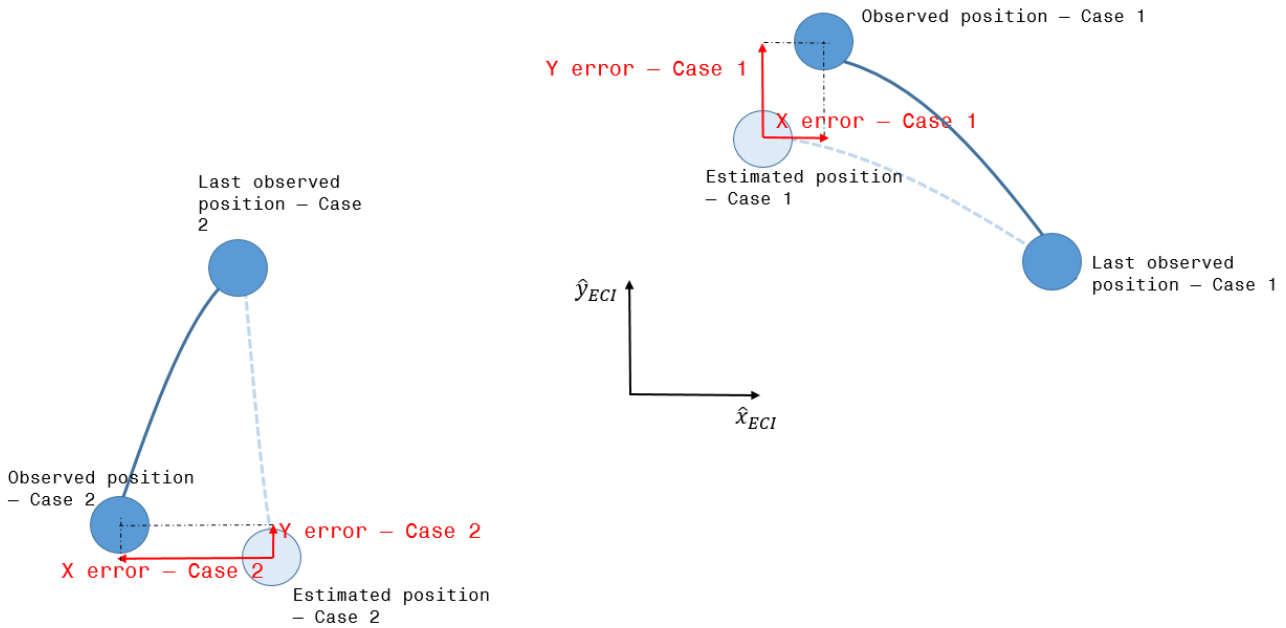


Figure 17: Two-dimensional sketch that shows how the errors may differ greatly in the ECI frame even that a clear pattern is shown – the error tends to the center of the orbit.

is analyzed in order to obtain the mean error and standard deviation of the real and the predicted position of the object.

The data of every object is known through the TLE files as the mean orbital elements for a given epoch, and there is usually updated Two-Line information every one or two days. In any case, this is not a rule and the elapsed time between measurements can vary greatly. The analysis is then performed in terms of the time between observations, as larger time gaps between measurements will give larger errors, as expected.

Both the position and the velocity for every TLE are in the ECI frame, which must be corrected. As Figure 17 shows, if the tendency of an object is to have an error between the estimated and real positions towards the exterior of the orbit, depending on its position in a given epoch, that error would be translated in a different combination of x, y, z errors depending on where in the orbit the observation was done. Even with a clear pattern, keeping the analysis in the ECI frame would not be useful.

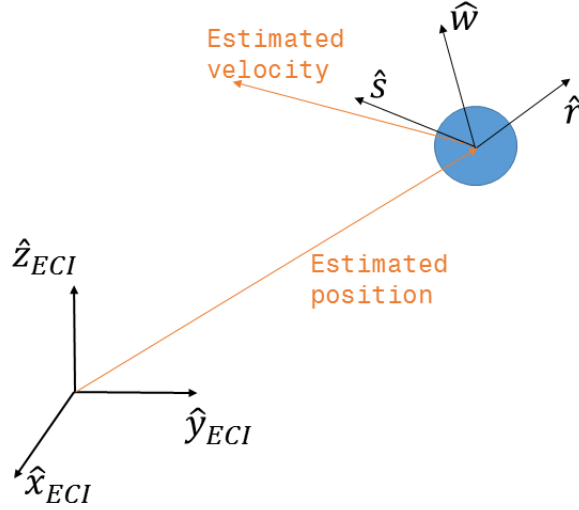


Figure 18: RSW coordinates frame.

In order to solve this problem a new reference frame is defined. This frame is centered onto the estimated position of the object, as it is the information the observer will have when preparing to make an observation, and it is related with the estimated velocity direction and position vectors in a *RSW* frame way, a coordinate system linked to a satellite explained by Vallado (2001)[5].

As seen in Figure 18, the \hat{r} direction is in the estimated position vector direction. The \hat{w} direction is in the estimated angular momentum direction, perpendicular to both the estimated position and velocity vectors. Finally the \hat{s} direction is perpendicular to both \hat{r} and \hat{w} , being more or less in the estimated velocity vector: for a perfect circular orbit, the \hat{s} vector would have the direction of the estimated velocity.

$$\hat{r} = \frac{\vec{r}_{est}}{r_{est}} \quad (1)$$

$$\hat{w} = \frac{\vec{r}_{est} \times \vec{v}_{est}}{|\vec{r}_{est} \times \vec{v}_{est}|} \quad (2)$$

$$\hat{s} = \hat{w} \times \hat{r} \quad (3)$$

The change of coordinates is applied for a pair of old-new TLEs, and five to seven years historical data is processed in order to have reliable results. Finally the mean error and the standard deviation are computed.

5.2 Statistical analysis

5.2.1 Introduction

In order to develop a cooperative targeting platform, a statistical analysis of the error between the estimated and the observed positions is done. Data from different Earth orbiting objects for a five to seven year period is obtained from the Space-trak website.

This historical information for more than 16,000 objects has been processed. The most important result is that the error along $\hat{\mathbf{s}}$ –which is the main direction of the velocity– is much higher than the error in the other directions. One particular example is shown in Figure 19, where it can be seen how for the #30,000 debris object of the catalog the error is mainly in the $\hat{\mathbf{s}}$ direction, while in the other two directions it's much smaller. Figure 19 shows how, for a day without observed data, errors up to almost 50 km can happen along the velocity direction, and around 15 km in the other directions. Sometimes a debris is not tracked for some days, causing the cumulative error to grow.

Since the purpose of this study is to provide a tool with which the AAs can cooperate to perform observations, data in terms of arcminutes or degrees is better suited for the Field of View of a telescope. This distance-to-angle transformation is done based on the altitude of each object above ground, and the $\hat{\mathbf{s}}$ direction is considered on-track, being the $\hat{\mathbf{w}}$ direction off-track. The altitude is assumed to be the semi-major axis, which is a characteristic distance of each object orbit, even that for eccentric orbit the altitude varies depending on the true anomaly at a particular epoch. Also, this analysis considers that the observer is directly below the object (in the line that connects the object and the center of the Earth), which will not be the majority of the case. Anyway, the results expressed in angular values are easy to comprehend and the simplifications done won't affect the general purpose of the study.

Object 30000 analysis, $a=41987.658\text{km}$
632 observations from 2012 to 2017

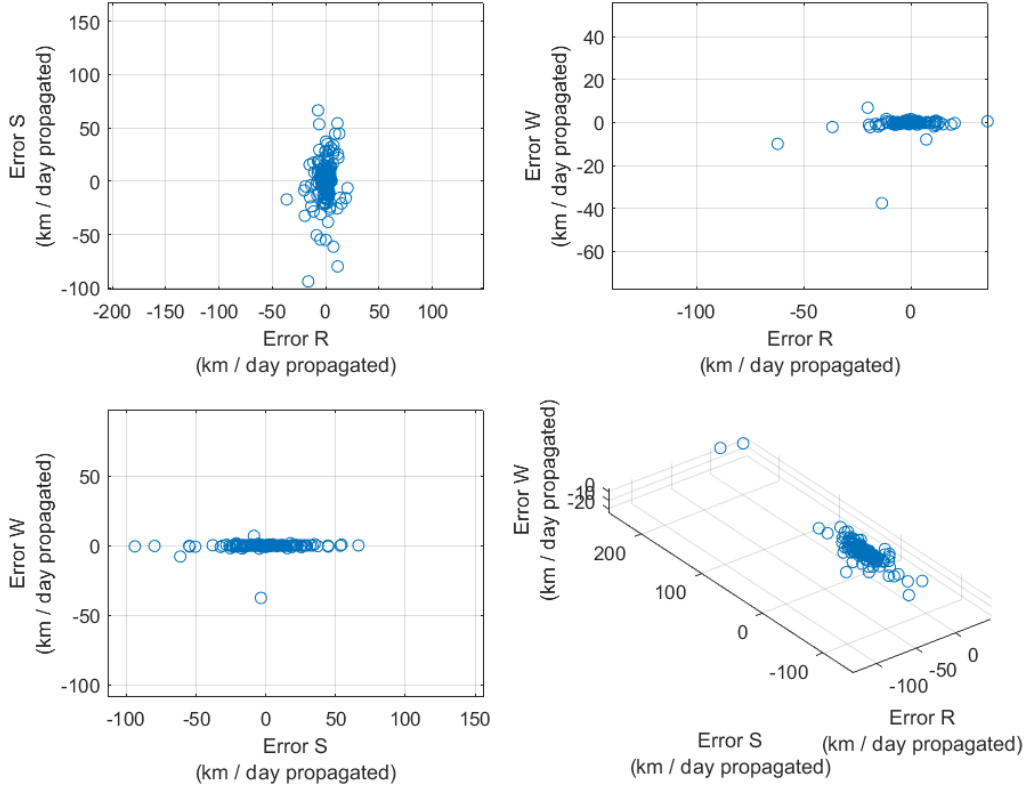


Figure 19: Debris object #30,000 of the catalog statistical analysis for a 5 year-period. Error between propagated and real positions in the RSW coordinates frame. 632 total TLE entries processed.

Considering a FOV of 30 arcmin, Figure 20 shows a characteristic ellipse of the object #30,000. This ellipse contains all the statistical information of the object. For each axis, the ellipse is centered in the mean error in that direction, and the semi-major and semi-major axis are set considering a ± 2 times the standard deviation of the error in each direction.

It can be seen how, for this object, the mean error is almost 0 in both axis. \hat{s} and \hat{w} are basically the along-track and cross-track directions, so taking into account the $\pm 2\sigma$ consideration, observation of this object will probably be a success, at least in terms of the real-to-predicted position deviation, if the time since the last observation is not more than a day, as in the \hat{w} direction (cross-track) the error is really small, and in the \hat{s} (along-track) even that it is higher it does not reach $pm0.5$ FOV per day of propagation.

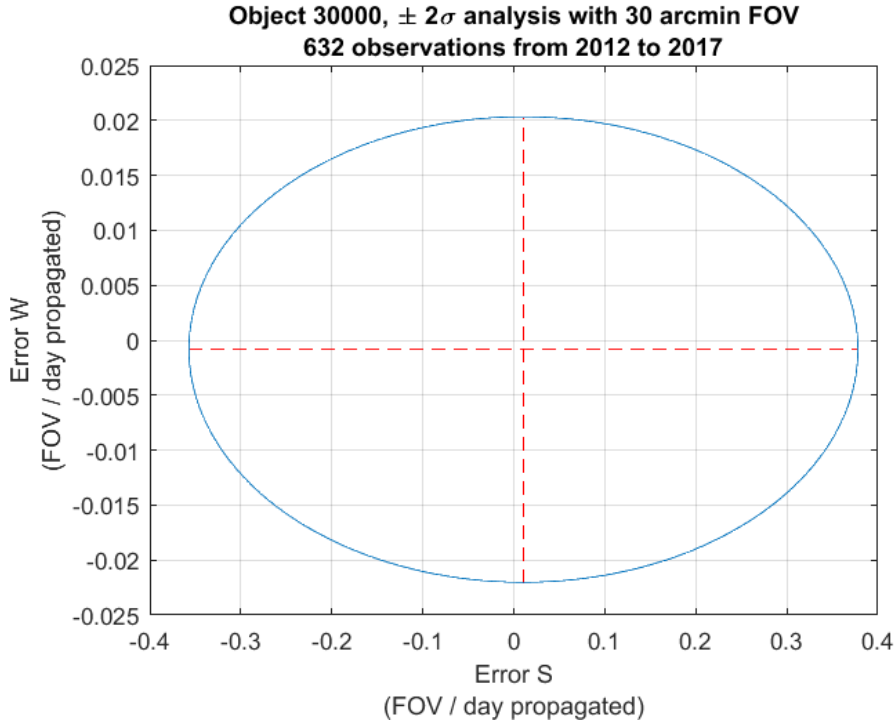


Figure 20: Characteristic ellipse of the debris object #30,000 of the catalog.

Every object of the catalog will have different deviation between the real and predicted position. In Figures 21 and 22 it is shown the analysis of the object #1,000 of the catalog. The ellipse shows how the errors in both axis are smaller than for the #30,000 object. However, in the \hat{w} direction the mean error is much higher and can't be neglected, especially since the propagation that needs to be done is higher than several days.

A final example is shown in Figures 23 and 24, which belong to object #4,864 of the catalog. This objects has much error than the other ones shown in this analysis, in both the $\pm 2\sigma$ term and the mean error (in the \hat{s} direction).

The information about the objects #1,000, 4,864 and 30,000 can be obtained in the Space-trak website and is contained in Table 4.

Table 4: Objects #1,000, 4,864 and 30,000 information

	Name	Launch	Incl (deg)	a (km)	ecc
#1,000	Titan 3A Deb	1965-02-11	32.14	2,790.5	0.00
#4,864	Thorad Agena D Deb	1970-04-08	99.5	1,078	0.03
#30,000	Titan 3C Transtage Deb	1968-09-26	6.09	35,609	0.01

Object 1000 analysis, $a=9173.423\text{km}$
 1184 observations from 2015 to 2017

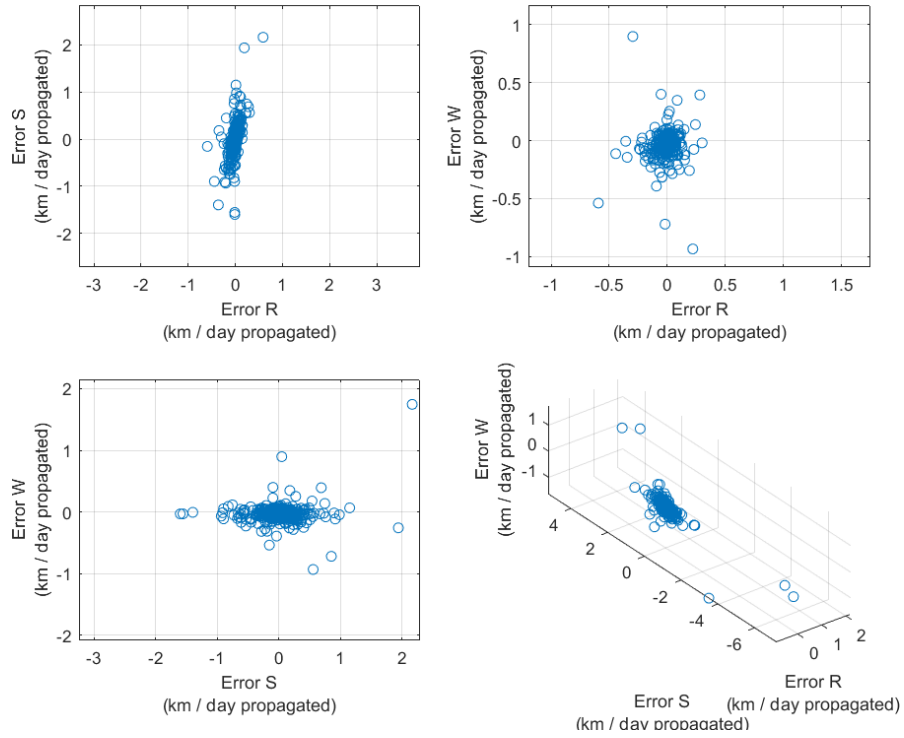


Figure 21: Debris object #1,000 of the catalog statistical analysis for a 5 year-period. Error between propagated and real positions in the RSW coordinates frame. 1,184 total TLE entries processed.

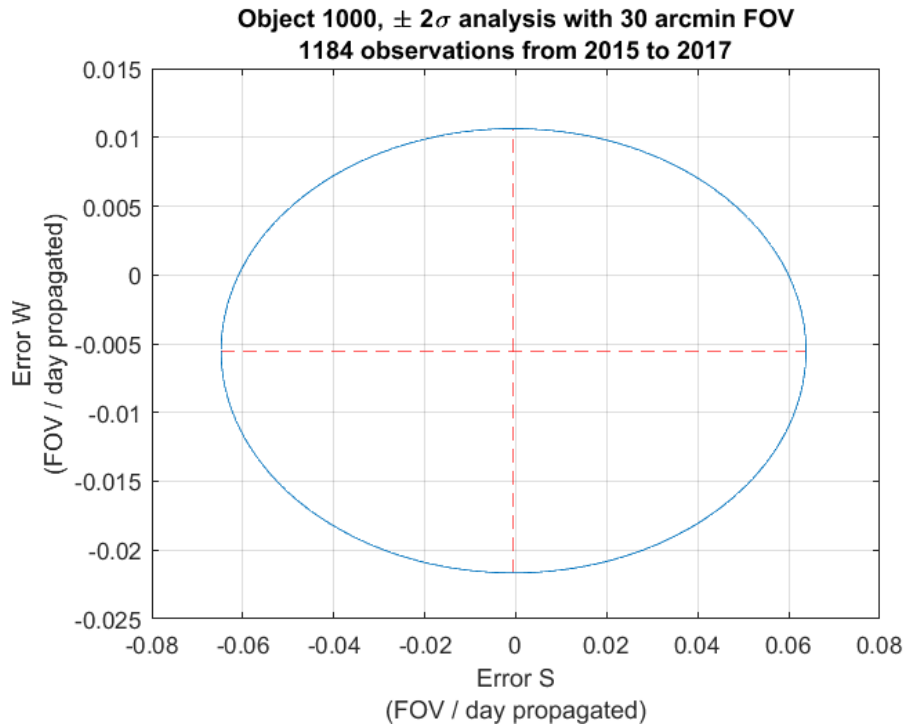


Figure 22: Characteristic ellipse of the debris object #1,000 of the catalog.

Object 4864 analysis, $a=7448.661\text{km}$
 1444 observations from 2015 to 2017

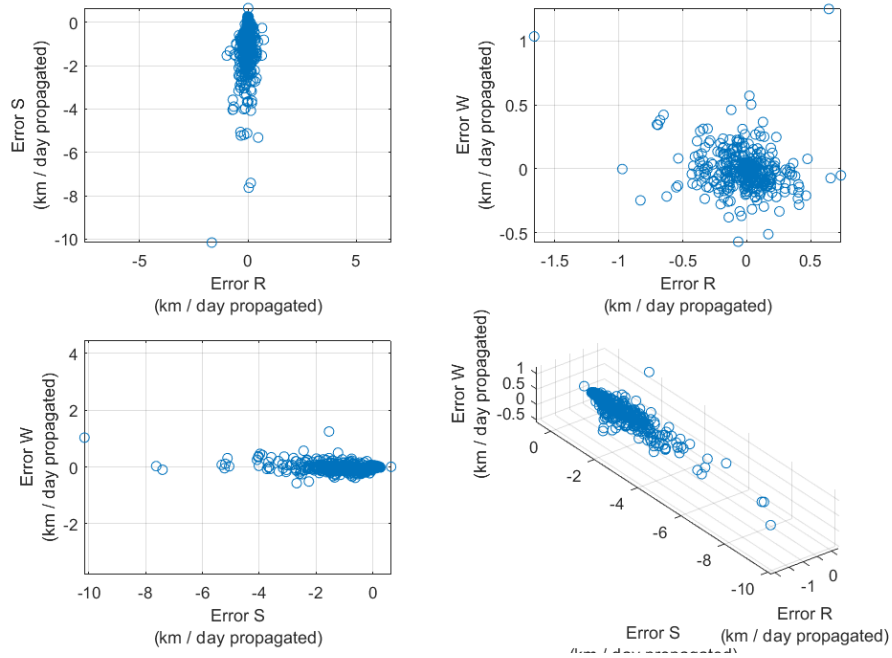


Figure 23: Debris object #4,864 of the catalog statistical analysis for a 5 year-period. Error between propagated and real positions in the RSW coordinates frame. 1,444 total TLE entries processed.

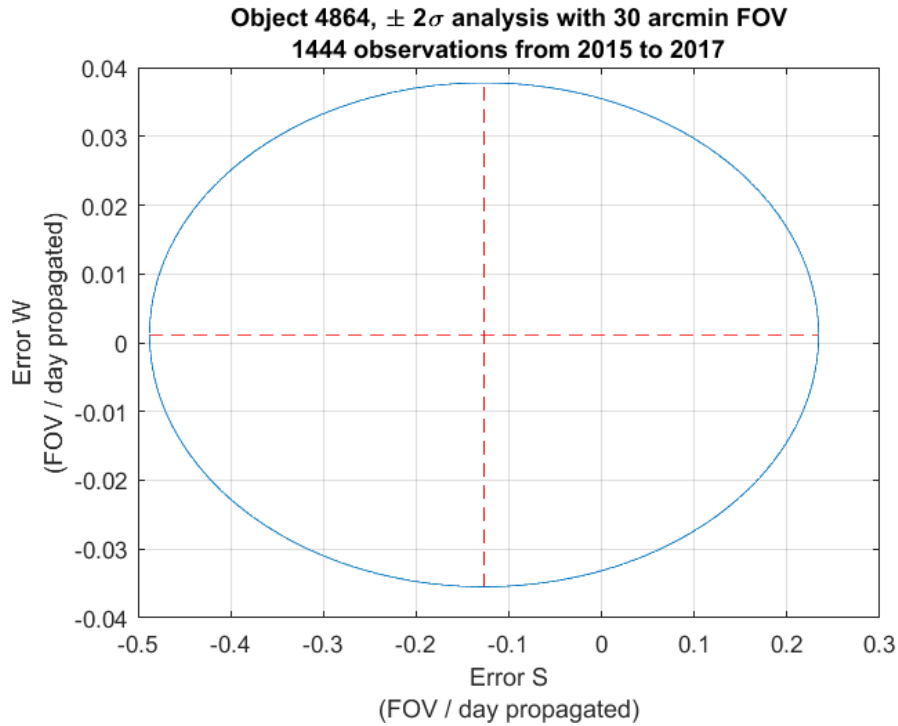


Figure 24: Characteristic ellipse of the debris object #4,864 of the catalog.

5.2.2 Global results

The global results of the statistical study are shown in Figure 25, where a total of 16,053 Earth orbiting objects are analyzed. For each object an ellipse is plotted, centered in the mean error and with semi-minor and semi-major axis of double the standard deviation of the error in that direction. \hat{s} and \hat{w} have been renamed to Along track and Cross track, as explained before.

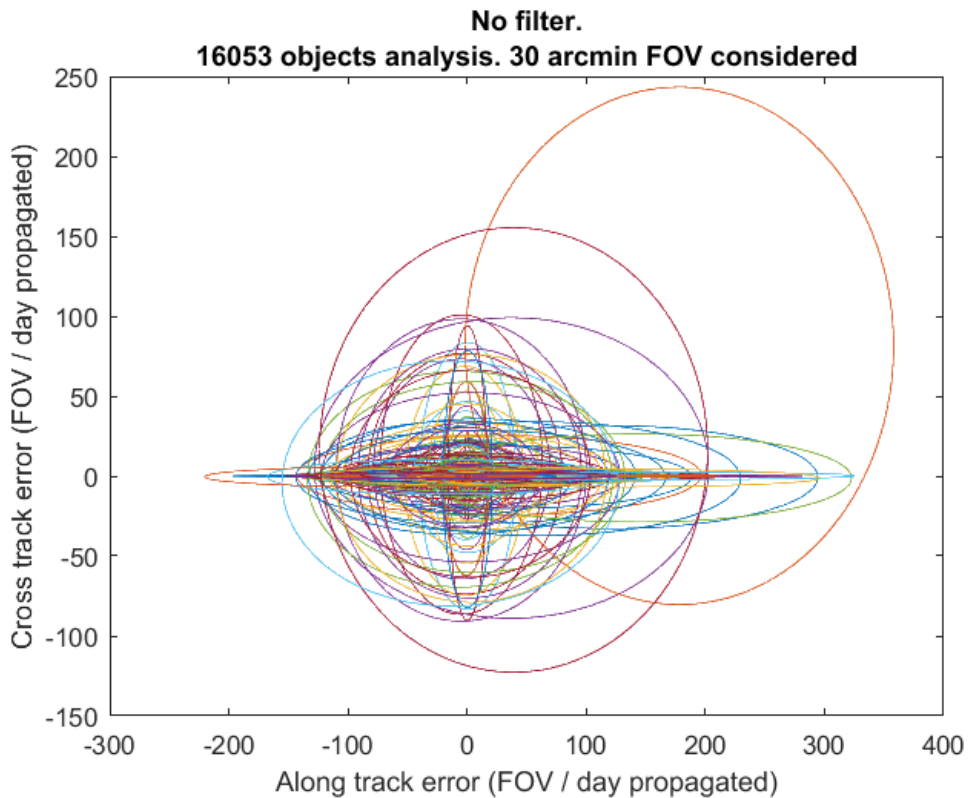


Figure 25: $\pm 2\sigma$ characteristic ellipses of 16,053 objects (almost all the current objects of the catalog).

It can be seen that there are some objects with high errors. These objects are considered outliers for the overall statistical analysis, as it will be shown later. The reason of these high errors is mainly in the TLE file. For the majority of the objects there is information about observations with a more or less regular frequency, but there are some objects that have irregular measurements, really big or small gaps between observations, repeated TLEs, etc. These issues are related with the source (NORAD, Space-trak, etc.) so the causes will not be analyzed further in this phase of the project. To prevent that they affect the

analysis significantly, an initial filter is applied when computing the object’s information.

Some other filters have been applied to have a better understanding of how the error behaves:

- No filter: all the 16,053 objects stored (Figure 25)
- Large errors: filtering of the objects with errors higher than $\pm 20 \text{ FOV/day}$ in the along-track direction and $\pm 5 \text{ FOV/day}$ in the cross-track direction (Figure 26)
- Observations: filtering of the objects from which there are less than 500 observations compared (Figure 27)
- Combination of large errors and observations: filtering both the large errors as described previously and also the objects with less than 500 observations (Figure 28)
- Reasonable errors: filtering of the objects leaving the ones with reasonable errors, selecting a threshold of $\pm 5 \text{ FOV/day}$ in the along-track direction and $\pm 0.5 \text{ FOV/day}$ in the cross-track direction (Figure 29)
- FOV-size errors: filtering of the objects leaving the ones whose errors don’t exceed 1 FOV in both directions (Figure 30)

A summary of the objects that pass each filter is shown in Table 5.

Table 5: Number of objects that pass the filters applied to the characteristic ellipses.

Filter	Number of objects	% of the total
No filter	16,053	100%
Large errors	15,801	98.43%
<500 observations	13,764	85.74%
Combined	13,632	84.91%
Reasonable errors	13,884	86.48%
FOV-size errors	8,547	53.24%

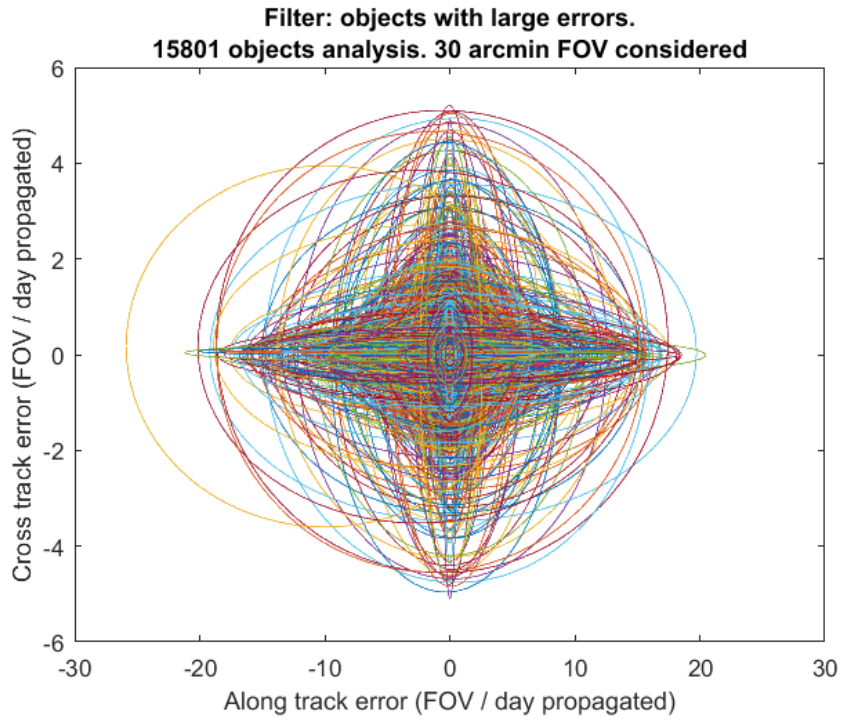


Figure 26: $\pm 2\sigma$ characteristic ellipses after filtering really high errors.

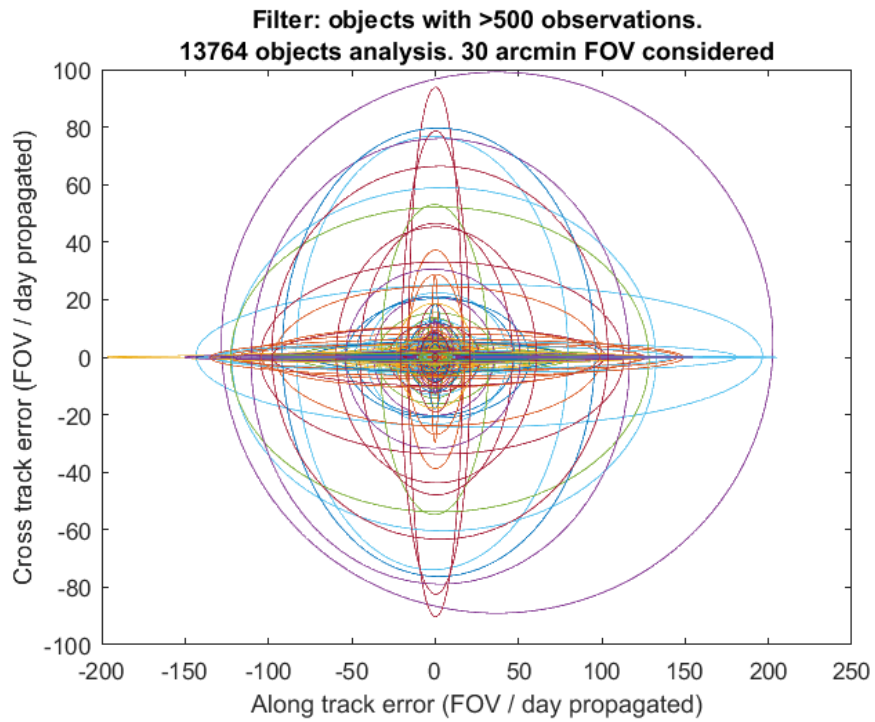


Figure 27: $\pm 2\sigma$ characteristic ellipses after filtering the objects with less than 500 observations.

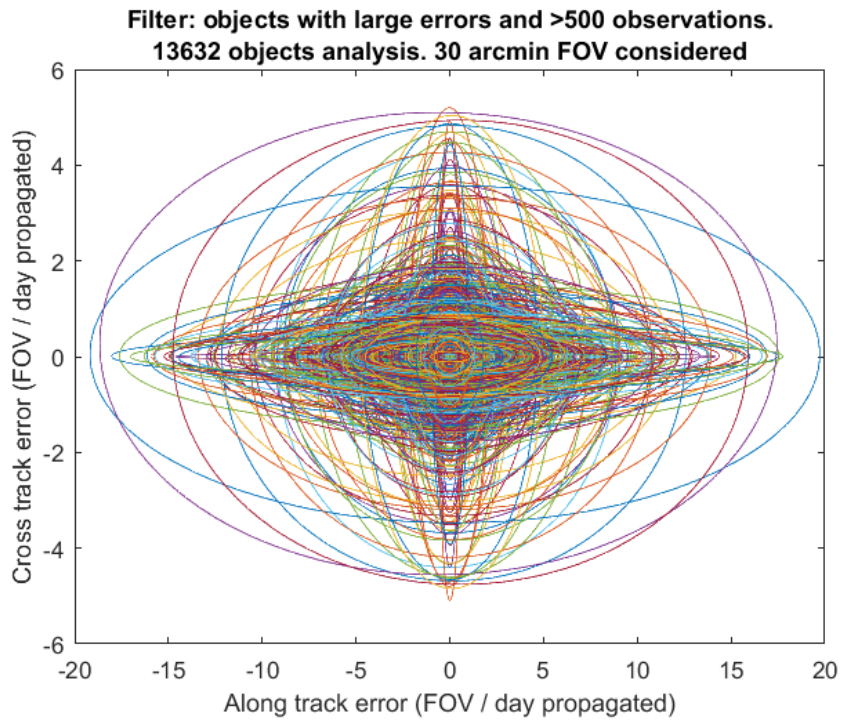


Figure 28: $\pm 2\sigma$ characteristic ellipses applying a combined filter that deletes high-error objects and less than 500 observations ones.

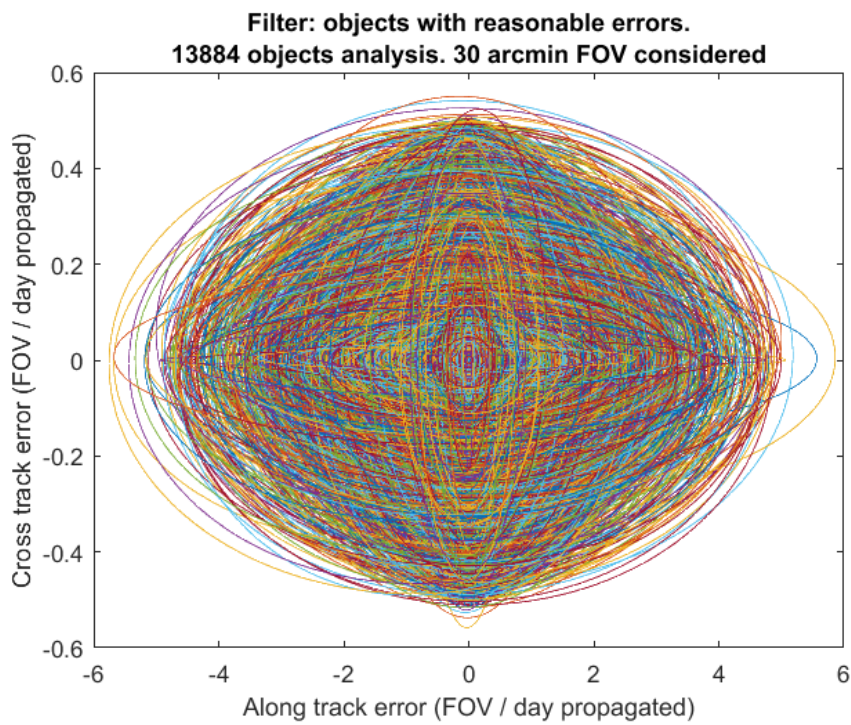


Figure 29: $\pm 2\sigma$ characteristic ellipses of objects with reasonable errors.

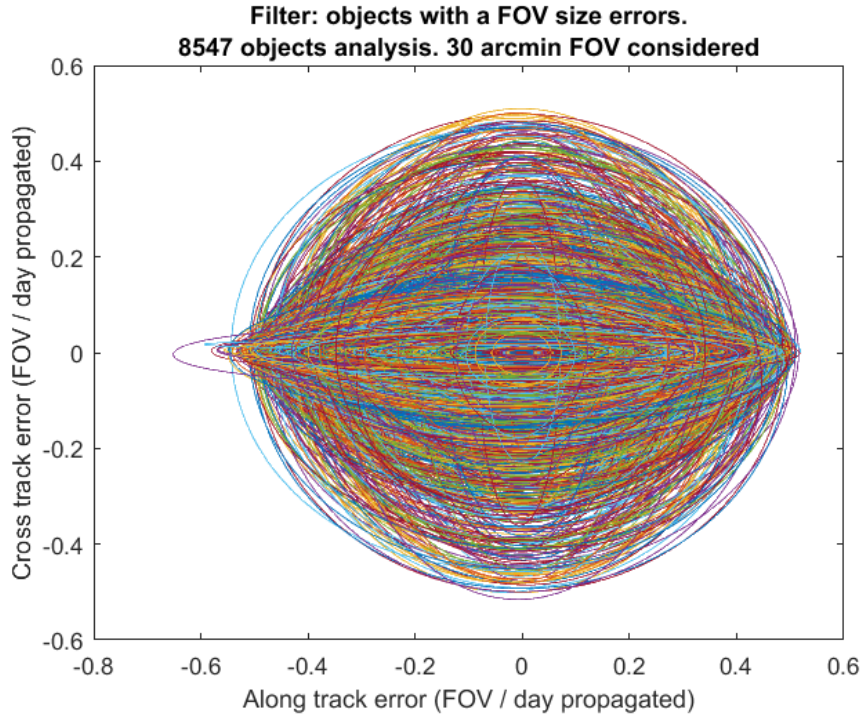


Figure 30: $\pm 2\sigma$ characteristic ellipses of objects with a maximum 1-FOV errors.

It can be seen how not too much objects have extremely large errors. The first filter applied just takes 1.57% of the objects from the analysis.

Having a small numbers of observations does not imply to have low or high errors, as the comparison of the combined filter shows. After filtering the objects with less than 500 observations recorded the number of objects decrease in almost 15%, but really high errors are still present, as the graph shows. Some of the objects are *young* (they have been launched recently), and that is the reason they don't have too much observations. An analysis between the number of observations and the lifetime could be done in order to locate the objects that have an small number of observations based on the time they have been in space.

Most of the objects (86.48%) have reasonable errors. That means they could be observed successfully in a single observation in terms of the cross-track direction and in no more than 10 observations in the along-track (Figure 29).

Finally, more than half of the objects (53.24%) could be located successfully

in a single observation, which is a promising result from the project. Even not having any information about a debris object that wants to be observed, there is an approximately 50% chance that the predicted position would be enough to do a successful observations (besides other kind of problems) if the time since the last TLE is not more than 1 day.

Note that all the errors are based on the propagation time, which is usually no more than 1 day as said before, and that several simplifications have been considered in order to measure the errors in terms of FOV.

5.2.3 Type of orbit

The last step of the study is a comparison of the errors depending on the orbit. The objects have been classified in 3 types with respect to their orbit:

- Low Earth Orbit (LEO): semi-major axis lower than 8,378 km, which is an altitude lower than 2,000 km (Figure 31)
- Medium Earth Orbit (MEO): semi-major axis higher than 8,378 km but lower than 40,000 km (Figure 32)
- High Earth Orbit (HEO): semi-major axis higher than 40,000 km (Figure 33)

This analysis does not take into account the eccentricity or inclination of the orbits. There are some high eccentric orbits that may fall into the MEO category even having a really small perigee altitude or a really high apogee altitude. Even that, the semi-major axis has been considered as a good parameter for the classification.

The first result from the analysis is about the number of objects in each category (Table 6). Most of the debris from the catalog are in LEO (78%), then in MEO (13.95%) and finally in HEO (8.05%). These numbers are important

because LEO objects are the fastest ones: they usually cross the FOV of a telescope in several seconds (or less than a second).

Table 6: Number of objects in the catalog per type of orbit.

Orbit	Number of objects	% of the total
LEO	12,522	78%
MEO	2,240	13.95%
HEO	1,291	8.05%

In Table 7 they are shown the average value of the errors for each type of orbit. The average values of the 16,053 objects show that a random object will be able to be captured in 4 observations, as the cross-track direction is fits inside a FOV, if the propagation is lower than a day.

The LEO objects are the ones with lower errors (below 3 FOV/day in the along-track direction), and the errors increase with the orbit's altitude. The mean errors are negligible: the $\pm 2\sigma$ term drives the error.

Table 7: Average error for each type of orbit.

(Errors in FOV/day of propagation and considering a 30 arcmin FOV)

	Mean along-track	$\pm 2\sigma$ along-track	Mean cross-track	$\pm 2\sigma$ cross-track
All objects	0.072	3.793	0.007	0.844
LEO	0.049	2.783	0.007	0.662
MEO	0.191	7.014	0.012	1.441
HEO	0.086	7.996	-0.002	1.578

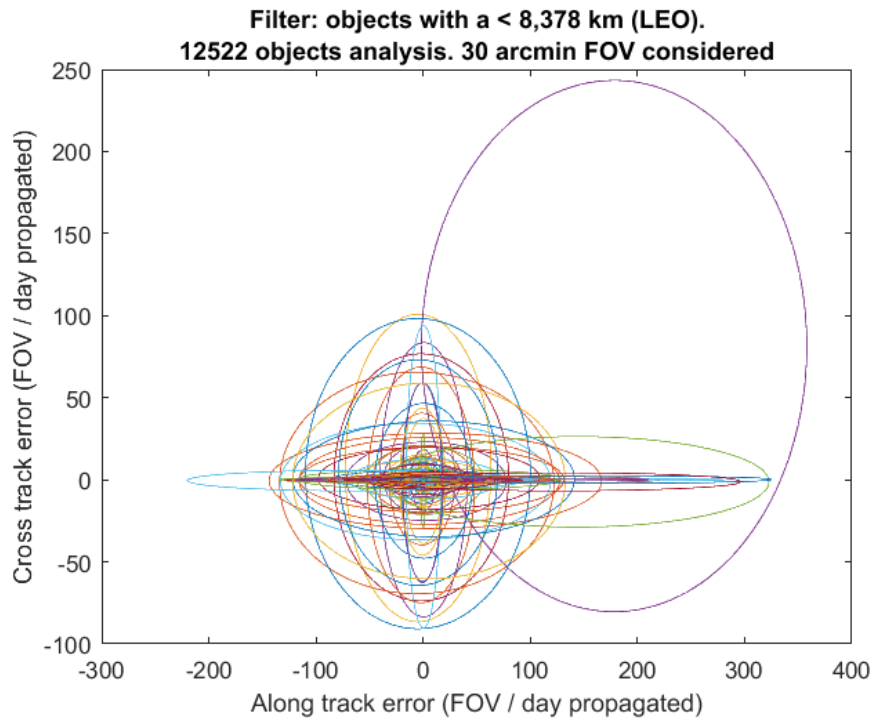


Figure 31: $\pm 2\sigma$ characteristic ellipses of LEO objects.

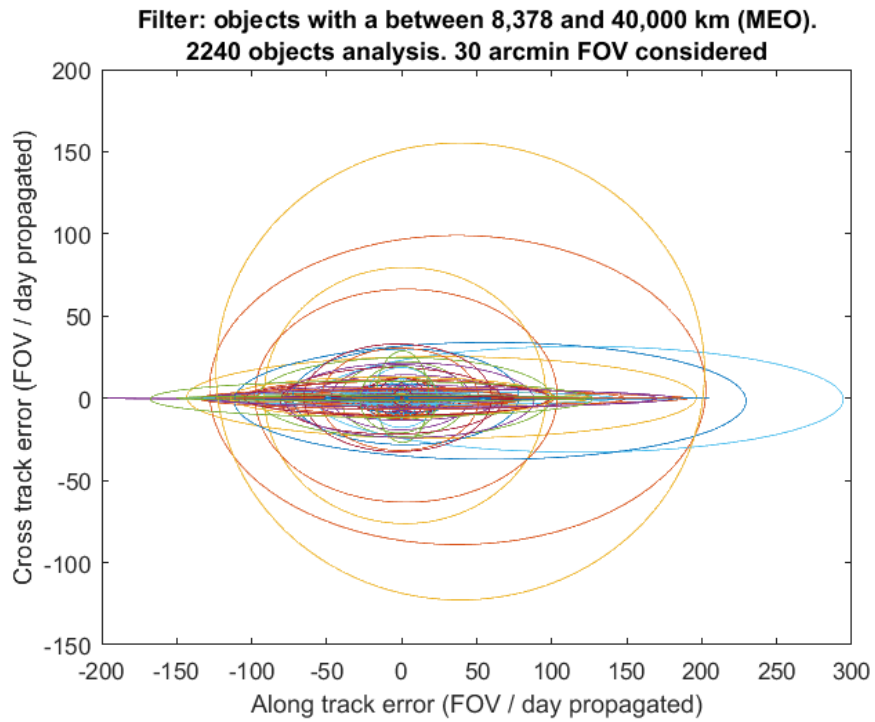


Figure 32: $\pm 2\sigma$ characteristic ellipses of MEO objects.

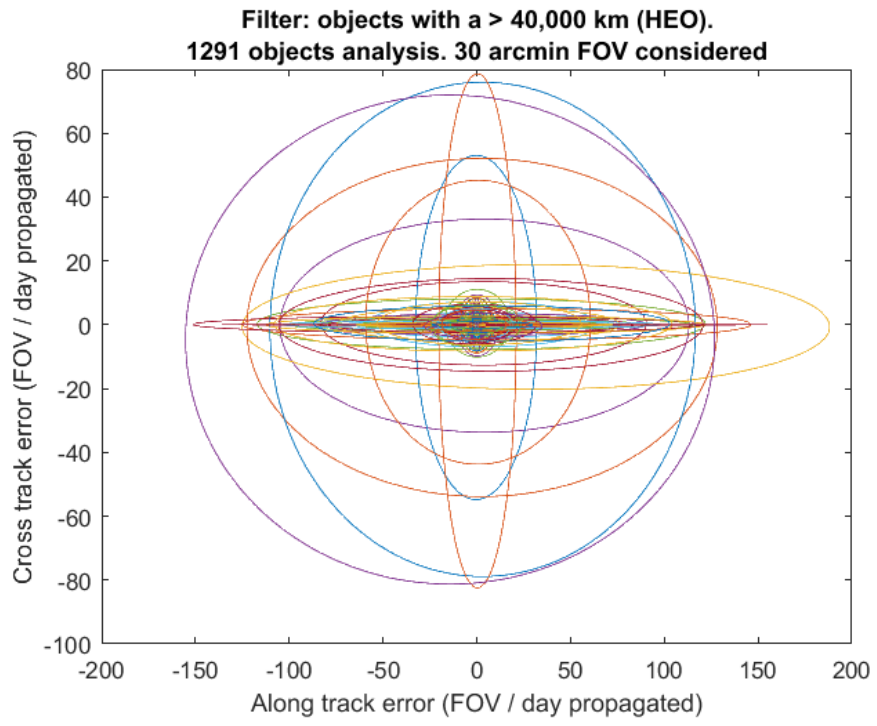


Figure 33: $\pm 2\sigma$ characteristic ellipses of HEO objects.

Chapter 6

Final Platform

The contribution of this thesis to the DCAP is contained in the folder *matlab_files*. At the same time, Angel Benedicto¹ has also worked in the project and has his own additions to it. Some of the work developed by Angel Benedicto is included in the folder *matlab_files*, as it is needed in other functions.

The MATLAB code and other files are distributed in both the main folder and several subfolders:

- `constraint_process.m`
- `tle.txt` files
- `README.txt`
- Subfolders
 - *Geometry*
 - *Historical_TLE*
 - *SGP4_files*
 - *TLE_files_storage*

6.1 Main folder

In the main folder there are several files: several `tle.txt` files, the MATLAB function `constraint_process.m` and a `README.txt`. Additionally it might be a `sat.mat` file and a `Untitled.m`.

¹Contact: angelbenedictoelena@gmail.com

The README.txt file is just a short guideline about the content of the folder. This document offers a much more detailed explanation, and all the important MATLAB files are commented for ease of use.

The tle.txt files are just single day TLE files from space-trak.org, that delivers each day a new file with all the new TLE entries. They are text files with around 30,000 to 40,000 lines, which means between 15,000 and 20,000 satellite records. The numbers in the name of the files indicate the day of the update. The first 4 digits are the year, the next 2 the month and the final 2 the day. For example, tle20170608.txt is the file containing all the TLE information recorded on June 8th 2017.

`constraint_process.m` is one of the main functions developed for the project. This function takes the location of an observer and a desired observation epoch and propagates a TLE file, applies the geometric constraints and selects one object to be observed. It also takes into account the time zone of the observer (as the TLE information is in UTC) and the FOV of the telescope. The output includes the RA-DEC coordinates of the observation, the exposure time of the image, the calibration star and the distance from the observer at the time of the observation. `Untitled.m` is just a basic example script that executes `constraint_process.m`.

`constraint_process.m` takes a complete TLE file provided by Space-trak, preferably the most recent one, and propagates all the position of all the objects until the desired epoch. Since propagation takes around two minutes, the object information at the desired epoch is stored in `sat.mat`, reducing the computation time for additional observations planned for the same epoch.

There are several features that still need improvements. At the time of this thesis, the exposure time was selected to be half of the time the object would take to cross the input FOV, and the observation is always centered on the predicted position. Ideally, a more exhaustive study could be done to take

the historical information and change both the pointing and the exposure time depending on it, and also taking into account if there have been previous recent failed observations of that object.

Also the calibration star selection just takes into account the 30 brightest stars, which is not enough. Angel Benedicto is working on improving this calibration.

6.2 Geometry folder

In this folder there are several functions, mainly developed by Angel Benedicto, that include all the geometric constraints, the calibration star selection and coordinates manipulation. They are mainly used by `constraint_process.m` and its complementary functions.

6.3 SGP4_files folder

This folder contains all the functions that are needed to perform the SGP4 propagation, fundamental to the operation of the project. These files have been developed by Jeff Beck² based in the previous work by Vallado and other authors.

6.4 TLE_files_storage folder

This folder contains all the TLE files used for the project and the necessary tools to download them.

The objective is to download historical TLE files from particular objects. Each files is referred to a particular object and will be named `tleXXXX.txt`, where the XXXX represent the number of the catalog of that object. In each files there will be all the TLE entries of that object in a given time span, which

²Contact: beckja@alumni.lehigh.edu

for this project has been set in 5-7 years. Even that, not all the objects have recent 5-to-7 year information, as they can be young or undiscovered until most recent times.

The files can be downloaded through the Space-trak website (<https://www.space-track.org/>). For that a user and a password are needed. Doing the downloads manually would take a lot of time: thankfully Space-trak has an API with which the downloads can be automated. A lot of information about the Space-trak API is in the website. The way it has been done for this project is using the software `wget`, which is present in the folder in the files `wget.exe`, `wget.exe.debug`, `wget.html` and `wget.ini.sample`³. Keeping these files in the folder will allow to perform the downloads from Space-trak using the PC Command Window.

A `.cmd` files has to be created in order to execute it with the Command Window and start the downloads. This `.cmd` files can be created through MATLAB. The function `get_tles.m` has been created for it, using an auxiliary function (`find_satnum.m`). `Untitled.m` provides an example of how to enter the inputs in the function `get_tles.m`, which are:

- TLEfile: a recent TLE file previously downloaded in Space-trak. It should be placed in the Main folder as explained previously
- user: Space-trak user email
- password: Space-trak user password
- end_date: maximum date for the TLE entries
- period: time span, in years, of the analysis
- exec: if 0, the function will end leaving a `.cmd` files in the folder. If 1, MATLAB will start the download of the `.cmd` directly

³Wget - GNU Project - Free Software Foundation <https://www.gnu.org/software/wget/>

The function will take the input TLE file and will look at the folder TLE_files, comparing which objects from the TLE file are already stored in the folder. After this it will take only the objects that are not already stored and will save a .cmd file ready to be executed (through MATLAB or directly in the Command Window).

The internal structure of the .cmd files is the following:

Space-track login:

```
wget - -post-data "identity=username@gmail.com&password=123456789abc"  
- -keep-session-cookies - -save-cookies=cookies.txt https://www.space-track.org/ajaxauth/login  
-olog
```

Download information:

```
wget - -limit-rate=100K - -keep-session-cookies - -load-cookies=cookies.txt  
https://www.space-track.org/basicspacedata/query/class/tle/EPOCH/2010-06-11  
- -2017-06-11/NORAD_CAT_ID/836/orderby/TLE_LINE1%%20ASC/format/tle  
-O C:/Users/Datos/Desktop/MARYLAND/THESIS/matlab/files/TLE_files_storage/  
TLE_files/tle836.txt
```

This line contains the time period of the download, the number of the catalog of the object and the location and name of the output .txt file.

Space-trak logout and delete auxiliary files:

```
wget - -limit-rate=100K - -keep-session-cookies - -load-cookies=cookies.txt  
https://www.space-track.org/ajaxauth/logout  
  
del log login logout
```

6.5 Historical_TLE

This folder contains the necessary MATLAB files to analyze the downloaded TLE files and process the information.

The MATLAB function *hist_analysis.m* takes the TLE files of the TLE_files_storage folder and creates a file *stat_tleXXXX.txt* for each object, that contains a comparison between real and predicted observations, as explained in previous chapters.

The MATLAB function *hist_read.m* takes the *stat_tleXXXX.txt* files created by *hist_analysis.m* and summarizes them in a single line of *histo.txt*.

histo.txt can be opened with MATLAB or Excel to be able to see the structure line by line. Each line contains the following information:

- Object's catalog number
- Number of observations of the analysis
- Semi-major axis of the object's orbit
- Time span of the analysis (last 2 digits of the start year, day of that year, last 2 digits of the end year, day of that year)
- Mean values of the error in the \hat{r} , \hat{s} and \hat{w} directions
- Standard deviation error in the \hat{r} , \hat{s} and \hat{w} directions

The MATLAB files *histo_process.m* and *stat_process.m* can be used to make plots or other analysis of the statistical files or the *histo.txt* summary file.

Chapter 7

Conclusions and Future Work

Improving the information about the objects orbiting Earth is essential to ensure the safety and reliability of future missions. The cooperation with the Amateur Astronomers community may be helpful for this purpose, and it has been demonstrated how with the correct tools this can be done.

The first condition is geometry. With the geometric constraints settled, almost 400 objects can be seen by an observer at a given position and time, which gives a lot of possibilities to fix a criteria with which select the most suitable one.

If there is a particular debris object of interest, cooperative targeting can be done in order to make sure that it is captured despite of the propagation errors, which can be of kilometers if the time since the last observation is long enough. With the historical analysis done, it has been demonstrated how the error between the real and the propagated position is mainly caused in the velocity direction, which will greatly simplify the coordination problem.

There are many other complications that have not been considered yet in this project:

There are a broad range of hardware systems (telescopes, targeting equipment, cameras) that are in use by the Amateur Astronomer community, and these have to be considered when developing processes for calibration and observation. When doing observations at the University of Maryland observatory it has been shown that capturing an object is much more difficult than expected.

Of the possible targets to be viewed, some may not be bright enough to be

observed by the equipment that is in use, so knowledge of the light gathering power of the equipment in use will be necessary. In general the brightness of the debris objects will be unknown, which makes difficult to know if a failed observation was caused by the lack of brightness or by other factors.

Many of the practical issues of making observations will manifest themselves as the developed procedures are tested at the University of Maryland Observatory.

Bibliography

- [1] Kelso, T. S., CelesTrak website <http://celestrak.com/>. Powered by the Center for Space Standards and Innovation (CSSI)
- [2] Hoots, F.R., and Roehrich, R.L., *Spacetrack Report #3: Models for Propagation of the NORAD Element Sets*. U.S. Air Force Aerospace Defense Command, Colorado Springs, CO, 1980.
- [3] Vallado, D.A., Crawford, P., Hujsak, R. and Kelso, T.S., *Revisiting Spacetrack Report #3*, presented at the AIAA/AAS Astrodynamics Specialist Conference, Keystone, CO, 2006 August 21–24.
- [4] Kelso, T.S., *Frequently Asked Questions: TLEs Format*. 2004, see <http://CelesTrak.com/columns/v04n03/>
- [5] Vallado, D.A., *Fundamentals of Astrodynamics and Applications*. Vol. 12. Springer Science & Business Media, 2001.
- [6] C. D. Hall, *Spacecraft Attitude Dynamics and Control* <http://www.dept.aoe.vt.edu/cdhall/courses/aoe4140/>